batteries

MDPI

Review

State of Charge and State of Health Estimation in Electric Vehicles: Challenges, Approaches and Future Directions

Babatunde D. Soyoye, Indranil Bhattacharya *, Mary Vinolisha Anthony Dhason and Trapa Banik

Electrical and Computer Engineering Department, Tennessee Technological University, Cookeville, TN 38505, USA; bdsoyoye42@tntech.edu (B.D.S.); mantonydh42@tntech.edu (M.V.A.D.); tbanik42@tntech.edu (T.B.)
* Correspondence: ibhattacharya@tntech.edu

Abstract: This critical review paper delves into the complex and evolving landscape of the state of health (SOH) and state of charge (SOC) in electric vehicles (EVs), highlighting the pressing need for accurate battery management to enhance safety, efficiency, and longevity. With the global shift towards EVs, understanding and improving battery performance has become crucial. The paper systematically explores various SOC estimation techniques, emphasizing their importance akin to that of a fuel gauge in traditional vehicles, and addresses the challenges in accurately determining SOC given the intricate electrochemical nature of batteries. It also discusses the imperative of SOH estimation, a less defined but critical parameter reflecting battery health and longevity. The review presents a comprehensive taxonomy of current SOC estimation methods in EVs, detailing the operation of each type and succinctly discussing the advantages and disadvantages of these methods. Furthermore, it scrutinizes the difficulties in applying different SOC techniques to battery packs, offering insights into the challenges posed by battery aging, temperature variations, and charge–discharge cycles. By examining an array of approaches—from traditional methods such as look-up tables and direct measurements to advanced model-based and data-driven techniques—the paper provides a holistic view of the current state and potential future of battery management systems (BMS) in EVs. It concludes with recommendations and future directions, aiming to bridge the gap for researchers, scientists, and automotive manufacturers in selecting optimal battery management and energy management strategies.

Keywords: electric vehicles; state of charge; state of health; battery management systems; electrochemical models; data-driven methods; machine learning

Academic Editors: Dongliang Chao and Harry E. Hoster

Received: 1 December 2024
Revised: 2 January 2025
Accepted: 13 January 2025
Published: 17 January 2025

Citation: Soyoye, B.D.; Bhattacharya, I.; Anthony Dhason, M.V.; Banik, T. State of Charge and State of Health Estimation in Electric Vehicles: Challenges, Approaches and Future Directions. *Batteries* **2025**, *11*, 32. https://doi.org/10.3390/batteries11010032

1. Introduction

Battery technology is a key challenge in the development of electric vehicles (EVs). Many countries, including the United States, have initiated special programs to increase battery performance to produce a battery system that can meet the criteria of EVs [1]. Battery cell performance has improved significantly thanks to the Several Year Plan like Battery500 Consortium and EV Everywhere Grand Challenge. Lithium-ion batteries (LiBs) and nickel metal hydride (Ni–MH) have been used in a wide range of EVs.

Effective battery management is critical for ensuring safe usage, extending operational longevity, increasing driving distance, fine-tuning power management strategies, and lowering battery costs.

A battery management system is made up of several types of communication lines, actuators, controllers, and sensors. Ensuring the safe and efficient utilization of battery

energy and furnishing precise battery status data to the vehicle energy management system constitute the fundamental functions of a BMS. It should also be able to provide the necessary interventions for the battery system if it is operating abnormally. Charging and discharging batteries are observed and managed for this purpose. Measuring current, voltage, and temperature by the gating signal received from the control circuit is the primary function of the sample circuit. With measurements of battery current, voltage, and temperature converted from the analog signal, the control circuit's primary job is to estimate the batteries' states of charge (SOC), health (SOH), available power capability (SOP), and life (SOL) using sophisticated algorithms. The vehicle controller receives these data, which include crucial decision-making elements for power distribution and energy management for vehicles [2,3].

The percentage of a battery's maximum possible capacity that remains is known as its state of charge or SOC. Battery SOC performs a function akin to that of a gasoline-powered vehicle's fuel gauge, indicating the remaining energy in a battery that powers an electric vehicle. Precise calculation of the battery, in addition to offering information about the battery's current energy and capacity, ensures a dependable and secure driving experience. However, estimating the state of charge (SOC) of batteries with some accuracy is a difficult process due to their complicated electrochemical nature, which exhibits diverse nonlinear behavior based on both external and internal factors. To meet the needs of electric vehicles (EVs), thousands of cells must be connected in corresponding series and in parallel due to the low voltage and energy of a single cell. Given the heterogeneous cell properties of operation and performance within each battery pack, predictions of the cells' inner occupied states continue to pose significant challenges. Furthermore, aging, temperature changes, and charge–discharge cycles all have a significant impact on battery performance, making it extremely difficult to estimate an exact state of charge [4].

Given the critical role that battery SOC plays in battery management, numerous approaches have been put forth to precisely determine the SOC. Scientists, researchers, and academics have been conducting in-depth studies since the early 1960s [5]. Nevertheless, there are not many publications that offer a thorough explanation of the main challenges in estimating battery SOC. Despite over fifty years of work, the problem of estimating the state of charge in batteries accurately has not been effectively resolved [6–8]. A thorough SOC estimation, including information on general research progress, future development patterns, and the origins of SOC estimation, has been provided by [7,9]. Nonetheless, a methodical explanation of the SOC computation procedure, algorithm selection, and handling of unpredictable environmental conditions and battery system grouping in electric vehicles is lacking. By examining various current approaches and addressing the major problems and difficulties for the SOC estimate of battery packs—rather than concentrating just on the battery cells—this research seeks to close the gap. Selecting the best battery management and energy management technique will be highly beneficial for the scientist, researcher, and car maker.

A taxonomy of the current SOC estimate techniques is presented in this research. It describes battery SOC estimate techniques in EV applications in a methodical manner, including every step of each type's operation. Comprehensive information about up-to-date SOC estimation techniques and difficulties is succinctly explained in Section 2. In Section 3, the techniques and difficulties associated with SOH techniques for battery packs are discussed. Section 4 discusses the key challenges faced in battery state estimation. Section 5 present the conclusion and recommendations.

2. SOC Estimation

As stated in the beginning, a battery management system's determination of its SOC is always a crucial component. The optimal design of the control system and vehicle energy management can be facilitated by a precise and dependable SOC estimation of a battery. As a result, SOC estimation is done in real-time using various techniques. We have divided these approaches into four groups to compare them in further detail: Figure 1 shows this division.

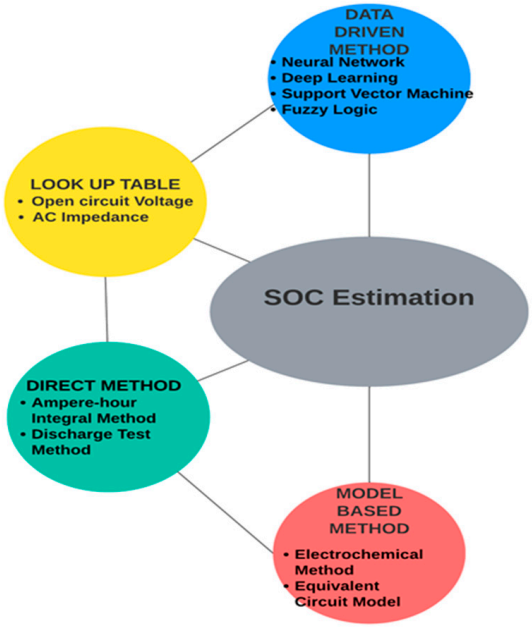

Figure 1. Classification of SOC estimation methods.

2.1. Look-Up-Table-Based SOC Estimation

This technique looks up the battery's terminal voltage on an "SOC versus open-circuit voltage (OCV)" curve after monitoring it when it is under load. This technique is based on the assumption that a cell model's terminal voltage equals the sum of the OCV and the voltage drop brought on by internal resistance and current. It finds the value on the "SOC versus OCV" curve after calculating OCV as a function of time. Although this is a step above the straightforward voltage-based approach, there are still several drawbacks [10], such as internal resistance (R_0) losses, diffusion voltages, and hysteresis among others that impact the accuracy of SOC estimations in batteries. The OCV curve may include some flat areas, as shown in Figure 2, in which it is challenging to calculate SOC with any degree of accuracy.

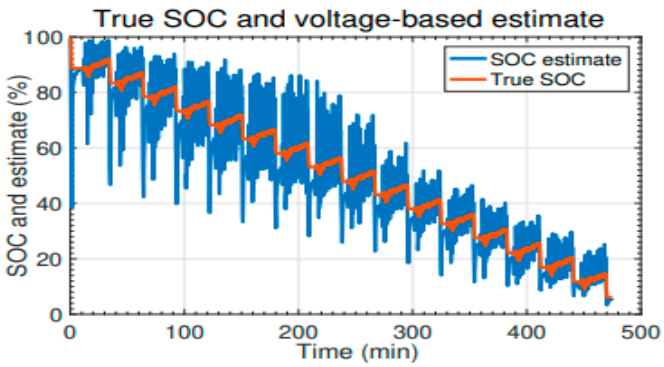

Figure 2. Open-circuit voltage curve.

It has been established that a nonlinear relationship exists between the SOC and OCV of a battery; as a result, estimating battery SOC by OCV after sufficient resting has grown in popularity and effectiveness and has been used in numerous applications [11,12].

The OCV approach can estimate battery SOC with excellent accuracy; however, a major drawback of OCV-based SOC estimation is the resting time. After cutting off the load current, it usually takes a while to regain equilibrium. Furthermore, changes in temperature affect the relationship between the SOC and OCV of a battery.

Due to its shortcomings, the open-circuit voltage (OCV) approach is not as appropriate for broad application in electric vehicles (EVs). Its impracticality for application in real-time scenarios, such as when the car is moving, is one of the main problems. The state of charge (SOC) of the EV battery might be estimated if it were possible to obtain the OCV data in real time while driving. This refers to being aware of the battery's remaining charge while operating the car, which is essential for organizing and arranging one's driving range [13]. The technique, like the voltage-based method, might not take hysteresis and diffusion voltages into full consideration.

In some circumstances, this approach may yield noisy SOC estimates, which reduces its accuracy.

Filtering can be used to increase estimate accuracy, but it may cause delays that should be considered for real-time applications.

Another challenging element that may impair the precision of SOC estimation is hysteresis, which is the reliance of a system's state on its past.

Notwithstanding these drawbacks, there are still situations where moderately noisy SOC estimates are appropriate or can be refined further to increase accuracy when using the look-up-table-based technique. When applying this approach to SOC estimation, it is critical to understand its limitations and possible causes of mistakes [10].

2.2. Direct-Based Method

2.2.1. Ampere-Hour Integral Method

This technique is used to determine a battery's state of charge. SOC stands for a battery's current state of charge, which is usually stated as a percentage.

$$\mathbb{SOC}(k) = \mathbb{SOC}(k_o) + \int_{k_o}^{k} \eta I(t) dt / C_n \quad (1)$$

$\mathbb{SOC}(k)$ denotes state of charge at time 'k', while $\mathbb{SOC}(k_o)$ denotes initial SOC (known estimate), η represents the efficiency of charging or discharging the battery, C_n is its nominal capacity, and $I(t)$ is the current being supplied to or drawn from the battery.

According to the formula, the starting SOC, current measurements, battery efficiency, and nominal capacity may all be used to determine the SOC at any given time 'k'. Efficiency factor η represents how efficiently a battery charges or discharges. This factor accounts for energy conversion efficiency losses that occur when the battery is being charged and discharged. Because it takes energy losses into account, it is a crucial parameter in SOC estimation. C_n is the battery's nominal capacity, which is the amount the manufacturer states it can hold. It serves as a benchmark for SOC computations. The technique depends on determining the amount of current (I) entering or leaving the battery. Charging is represented by positive current values, whereas negative values represent discharging. The accuracy of SOC estimation depends critically on the precision of current measurements.

Several difficulties with the ampere-hour (Ah) method of SOC estimation are mentioned in this paragraph. These difficulties consist of:

- Dependence on Current Measurements: The precision of current measurements has a significant impact on SOC estimation when utilizing the ampere-hour method. Inaccuracies in SOC estimates may result from current measurement mistakes.
- Error Accumulation: The accuracy of SOC estimates may be considerably impacted over time by inaccuracies in current measurements that accumulate.
- Difficulty in Determining Initial SOC: Accurately determining the initial state of charge (SOC) can be difficult in real-time applications, particularly if the battery is not fully charged or depleted. Precise SOC estimation requires accurate initial SOC.
- Calibration Challenges: Using the Ah technique for SOC estimation can present calibration challenges for both the original SOC and current readings. To take into consideration errors and variances in the system, calibrations are required.

In conclusion, the Ah method for estimating SOC is a simple technique that depends on current measurements; yet, it has issues with accuracy, accumulation of errors, and determining the initial SOC. Improving the accuracy of SOC estimates while utilizing this method requires addressing these issues.

2.2.2. Discharge Test Method

This approach is thought to be the most accurate for estimating SOC. The discharge test method is reliable [14,15]. The battery must be discharged at a constant current, and the product of the discharge current and time yields the SOC. This is a flexible approach that works with different kinds of batteries. It is frequently used in scientific settings to investigate battery charging, discharging characteristics, and maintenance as well as to define a benchmark for SOC accuracy.

The limitations of the discharge test approach are that it is time-consuming and not appropriate for determining SOC while a vehicle is in motion, despite its excellent accuracy. It therefore constitutes requires a laboratory process.

In conclusion, the classic direct-based method of estimation has the benefit of an algorithm that is straightforward to implement; however, due to the greater hardware requirements, a significant amount of experimental investment is required, and the method's performance is limited to estimating SOC.

The voltage-based method's accuracy rises with the battery's standby period, meaning that the test duration will be increased correspondingly, based on the features and accuracy of each method. The initial state-of-charge estimation is the primary application for the ampere-hour (Ah) integral approach. However, as test times increase, the accuracy of this method declines due to the continual changes in internal resistance caused by various factors. Although the discharge test method is quite precise, it can only be used in a laboratory setting and is not appropriate for use on actual automobiles.

2.3. Model-Based State Estimation

It is necessary to carefully create a good battery model for the model-based techniques. Battery equivalent circuit models [16] and electrochemical models [17,18] are typically used to estimate SOC in a battery, using state space. Subsequently, a range of state observers, including the sliding mode observer, Kalman filter (KF), and the extended, adaptive, and unscented Kalman filter are employed for online SOC estimation [19–22]. Training the battery models, selecting the right tools to monitor them, making important model settings, and fine-tuning the way we observe them using a particular method called the Kalman filter all have a significant impact on how accurate these model-based techniques are. It is presumed that the system has a mathematical model, as shown in Figure 3. The same input is spread throughout the model and real systems.

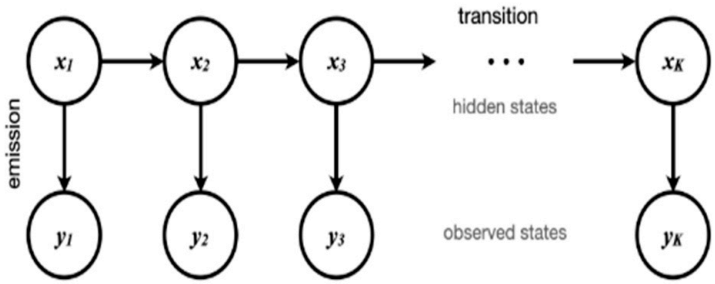

Figure 3. State transition diagram for a hidden Markov model.

Comparison of measured and expected outputs, use of error to update the model's estimation of the actual state measurement, and model mistakes can cause output errors. Careful updating is required to account for each of these. Furthermore, a trustworthy confidence zone is typically difficult to achieve, and the observer performance test of the SOC is done under given conditions. Consequently, it is impossible to guarantee the estimation performance under time-varied real-world circumstances that differ from the test conditions.

A generic flowchart of model-based SOC estimate techniques is displayed in Figure 4. These techniques are a subset of fusion techniques which involve the integration of different approaches with the OCV using the look-up table. It is observed that between the look-up table and ampere-hour methods, the SOC of batteries serves as a bridge. An erroneous battery OCV is caused by an inaccurate SOC estimate determined by the ampere-hour integral approach, which also raises the terminal voltage forecast inaccuracy. Thus, only after obtaining the optimal SOC can the battery terminal voltage prediction error be as low as possible. Stated differently, the estimation error can be corrected using the OCV.

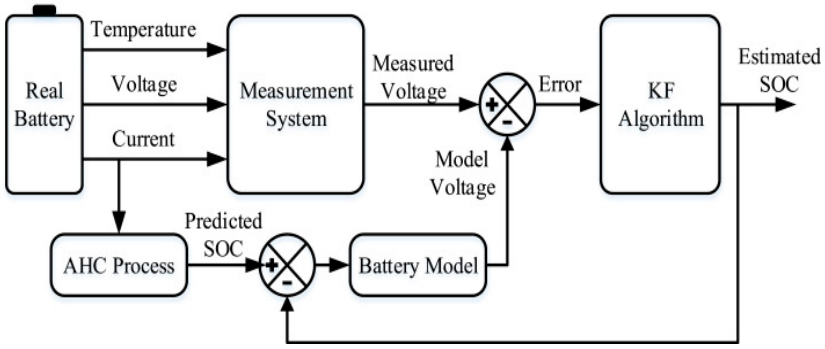

Figure 4. Flowchart of a model-based SOC estimation.

A particular example of sequential probabilistic inference is the Kalman filter, which provides the best state estimate under certain circumstances.

Linear Kalman filter and variations

Sequential Probabilistic Inference.

We start by assuming a general, possibly nonlinear model:

$$x_k = f\,(x_{k-1},\, u_{k-1},\, w_{k-1}) \tag{2}$$

$$y_k = h\,(x_k,\, u_k,\, v_k), \tag{3}$$

where u_k, w_k, and v_k are a measured input, process random, and sensor random input, respectively. We note that $f\,(.)$ and $h\,(.)$ are time-varying. Estimating the present state x_k of a dynamic system using $\mathbb{Y}_k = \{y_0,\, y_1 \ldots\, y_k\}$, we can "peep" at what is going on

in the actual system thanks to the observations. We estimate the state based on our model and observations, but randomness in process noise and sensor noise prevents us from ever being able to calculate the state exactly [23].

Review of probability

Noise is by definition random in some way; it is not deterministic. Hence, to discuss how noise affects system dynamics, it is necessary to comprehend "random variables" (RVs).

We are unable to precisely forecast the results of each measurement or sample of the random variable, but we can use the "probability density function" (PDF) to describe the probability of each sample value. Random vector X and sample vector x_0 are defined as:

$$X = \begin{bmatrix} X_1 \\ X_2 \\ \vdots \\ X_n \end{bmatrix}, \; x_0 = \begin{bmatrix} x_1 \\ x_2 \\ \vdots \\ x_n \end{bmatrix}, \tag{4}$$

where X_1 through X_n are scalar random variables, and x_1 through x_n are scalar constants.

X described by (scalar function) joint PDF $f_X(x)$ of vector X.

$f_X(x_0)$ means $f_X(X_1 = x_1, X_2 = x_2, \ldots, X_n = x_n)$. That is, $f_X(x_0)\, dx_1\, dx_2 \ldots dx_n$ is the probability that X is between x_0 and $x_0 + dx$.

There is an unlimited range of PDFs; however, while creating the Kalman filter, only the (multivariable) Gaussian PDF is utilized. It is assumed that all sounds and the state vector are Gaussian random vectors.

The Gaussian or normal PDF as presented in Figure 5 is defined as:

$$X \sim \mathcal{N}\left(\overline{x}, \sum \widetilde{X}\right) \tag{5}$$

$$F_X(x) = \frac{1}{\sqrt{(2\pi)^n |\sum X|}} exp\left(-\frac{1}{2}(x-\overline{x})^T \sum_{\widetilde{X}}^{-1} (x-\overline{x})\right) \tag{6}$$

where n is the dimensionality of the random variable X, $|\sum X|$ is the determinant of the covariance $\sum X$, and $(x-\overline{x})^T \sum_{\widetilde{X}}^{-1} (x-\overline{x})$ is the Mahalanobis distance measuring how far x is from the mean in terms of the variance.

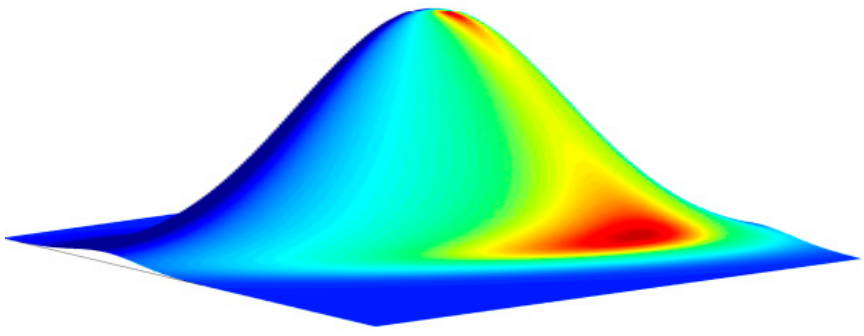

Figure 5. 3D Surface plot showing a single-peak distribution.

Linear Kalman Filtering

Kalman filtering theory was introduced in 1960 [24]. Consider the linear discrete-time system in Figure 6. The unit-delay operator is $z^{-1}I$, and the matrices A_k, B_k, and C_k are (possibly) time-varying. The system's deterministic input is u_k, and its output is y_k. Additionally, there are two stochastic inputs: measurement noise v_k, which does not affect

the state x_k, and process noise w_k, which does. Inferred, the system state, x_k, is an internal (hidden) signal.

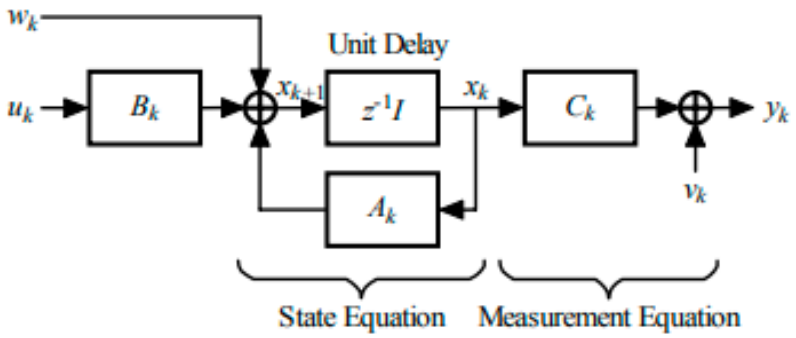

Figure 6. Block diagram showing SOC state estimation.

The foundation of Kalman's theory is the idea of the state. A system's state is the smallest possible collection of information needed to accurately characterize its unforced dynamics [25]. Stated differently, it is the minimum amount of historical behavior data needed to forecast future behavior. The status is usually unknown and might not be quantifiable. We must use observations on y_k to determine its value.

We may mathematically describe the system in Figure 6 with two equations. The state equation is:

$$x_{k+1} = A_k\, x_k + B_k u_k + w_k \tag{7}$$

The zero mean and covariance matrix is as follows:

$$E\left[w_n w_k^T\right] = \begin{cases} \sum w & n = k \\ 0 & n \neq k \end{cases} \tag{8}$$

Assuming that w_k is additive, white, and Gaussian.

The system's varying dynamic nature is captured by the state equation. This equation, for instance, can be used to determine system stability, dynamic controllability, and sensitivity to disturbance.

The second equation describing the system is the measurement equation:

$$y_k = C_k x_k + v_k \tag{9}$$

A linear combination of states is the output of the system at discrete-time k. Measurement noise also contributed to this output. Once more, measurement noise v_k is assumed by Kalman filter theory to be additive, white, and Gaussian, with zero mean and covariance matrix:

$$E\left[v_n v_k^T\right] = \begin{cases} \sum v & n = k \\ 0 & n \neq k \end{cases} \tag{10}$$

The Kalman filter problem is then: Use all of the observed data $\{u_1, u_2, \cdots, u_k\}$ and $\{y_1, y_2, \cdots, y_k\}$ to find the minimum mean squared error estimate $\hat{x}_k$ of the true state x_k. That is, solve:

$$\hat{x}_k = \text{argmin} E\left[(x_k - \hat{x}_k)^T (x_k - \hat{x}_k) \parallel u_1, u_2, \cdots, u_k, y_1, y_2, \cdots, y_k\right] \tag{11}$$

This problem has a well-known solution, which is shown in Equations (12)–(26) below. A series of recursive relationships that incorporate the covariance and an estimate of the state itself form the basis of the solution and the covariance matrix $\sum e,k$ of the state estimate error $x_k - \hat{x}_k$. The uncertainty of the covariance matrix is shown by the state estimation, and it might be applied to provide estimate error bounds. A "large" $\sum e,k$ (one with large singular values) suggests a high level of uncertainty in the estimate; a "small" $\sum e,k$ (one with small singular values) implies a significant level of confidence in the state estimate [26].

Summary of the Kalman filter from reference [27]:

State-space model:

$$x_{k+1} = A_k\, x_k + B_k u_k + w_k \tag{12}$$

$$v_k = C_k x_k + v_k \tag{13}$$

where C_k is the measurement matrix, and w_k and v_k are independent, zero-mean, Gaussian noise processes of covariance matrices $\sum w$ and $\sum v$ respectively.

Initialization: for $k = 0$, set

$$\hat{x_0^{(+)}} = E[x_0] \tag{14}$$

$$\sum\nolimits_{e,k}^{(+)} * = E\left[(x_0 - E[x_0])(x_0 - E[x_0])^T\right] \tag{15}$$

Computation: For k = 1, 2, … compute:

State estimate propagation:

$$\hat{x_k^{(-)}} = A_{k-1}\hat{x}_{k-1}\ (+) + B_{k-1}u_{k-1} \tag{16}$$

Error covariance propagation:

$$\sum\nolimits_{e,k}^{(-)} * = A_{k-1}\sum\nolimits_{e,k-1}(+)A_{k-1}^T + \sum\nolimits_w \tag{17}$$

Kalman gain matrix:

$$L_k = \sum\nolimits_{e,k}^{(-)} * C_k^T\left[C_k\sum\nolimits_{e,k}^{(-)} * C_k^T + \sum\right]^{-1} \tag{18}$$

State estimate update:

$$\hat{x_k^{(+)}} = \hat{x_k^{(-)}} + L_k\left[v_k - C_k\,\hat{x_k^{(-)}}\right] \tag{19}$$

Error covariance update:

$$\text{the } \sum\nolimits_{e,k}^{(+)} * = (I - L_k C_k)\sum\nolimits_{e,k}^{(-)} * \tag{20}$$

The Kalman filter is initialized with the best available information on the state and error covariance.

$$\hat{x_0^{(+)}} = E[x_0] \tag{21}$$

$$\sum\nolimits_{x,0}^{(+)} * = E\left[(x_0 - E[x_0])(x_0 - E[x_0])^T\right] \tag{22}$$

Although this initialization must frequently be done on the fly, the Kalman filter rapidly converges on the correct values as it operates.

After initialization, the Kalman filter repeats two actions. Initially, it predicts the error covariance, system output, and the value of the subsequent state. Second, it corrects the present state estimate based on a measurement of the system output $\hat{x_k^{(-)}}$ and $\sum\nolimits_{e,k}^{(-)} *$,

respectively, representing the estimated error covariance and predicted state at time index k but before the measurement. Following the measurement, the corrected estimations are indicated by $\hat{x}_k^{(+)}$ and $\sum_{e,k}^{(+)} *$.

The prediction step is accomplished by propagating the system through the system dynamics:

$$\hat{x}_{k+1}^{(-)} = A_k \, x_k^{(+)} + B_k u_k \tag{23}$$

The state uncertainty is also updated:

$$\sum_{e,k+1}^{(-)} * = A_k \sum_{e,k}^{(+)} * A_k^T + \sum w \tag{24}$$

If the system is stable, the first term is contractive, reducing uncertainty. The process noise always increases the uncertainty $\sum w$.

The state correction step is:

$$\hat{x}_k^{(+)} = \hat{x}_k^{(-)} + L_k \left[v_k - C_k \, \hat{x}_k^{(-)} \right] \tag{25}$$

In other words, the predicted state estimate plus a weighted correction factor equals the new state estimate. Subtracting the expected cell voltage from the measured cell voltage equals the term enclosed in square brackets [28].

Due to measurement noise, an erroneous state estimate $\hat{x}_k^{(-)}$, or an imprecise cell model, this term might not be zero. It is frequently referred to as the "innovation" process, as it symbolizes the "new information" in the measurement. A major innovation usually results in a large state update. A tiny innovation usually results in a small state update.

The innovation is weighted by the Kalman gain L_k:

$$L_k = \sum_{e,k}^{(-)} * C_k^T \left[C_k \sum_{e,k}^{(-)} * C_k^T + \sum v \right] \llbracket^{-1} \tag{26}$$

A significant update is required if the present state estimate is highly uncertain, as indicated by large values of the $\sum e, k$ and L_k. L_k is tiny, and the state-estimate update is minimal if the current state estimate is certain. Furthermore, a considerable amount of sensor noise results in a large $\sum v$, which in turn causes a small L_k and a small update.

The covariance correction step is:

$$\sum_{e,k}^{(+)} * = (I - L_k C_k) \sum_{e,k}^{(-)} * \tag{27}$$

The state uncertainty always decreases due to the new information provided by the measurement.

In Figure 7, the left-hand graph, titled 'Kalman filter in action', compares the true state of a system (solid line) against the estimated state provided by the Kalman filter (dashed line) across iterations. The magenta bounds represent the estimated uncertainty or confidence interval. The right-hand graph, titled 'Error with bounds', shows the estimation error (solid blue line) and its bounds (dashed magenta line), which likely represent the expected range of error, across the same iterations. These plots are instrumental in evaluating the accuracy and reliability of Kalman filter predictions over time.

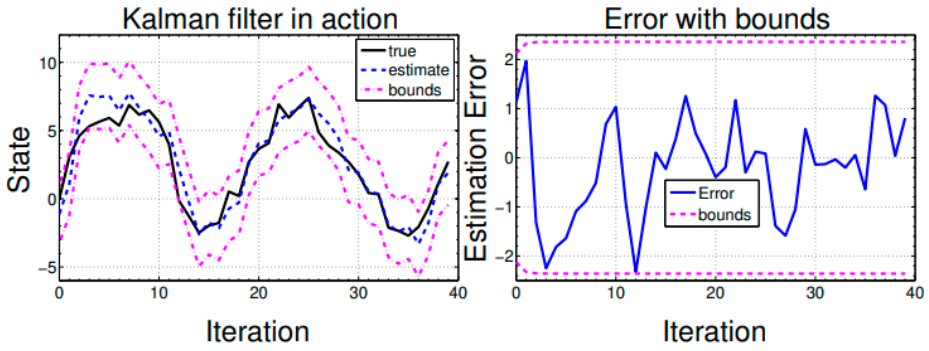

Figure 7. Performance analysis of a Kalman filter.

Extended Kalman Filtering

The Kalman filter is the best state estimator. In a nonlinear system, we can approximate the nonlinear system with a linear time-varying (LTV) system by using a linearization procedure at each time step. The extended Kalman filter (EKF) on the real nonlinear system is produced by using this LTV system in the Kalman filter. Keep in mind that while EKF is not always the best option, it frequently functions more effectively than others [28].

The nonlinear system may be modeled as:

$$x_{k+1} = f(x_k,\ u_k) + w_k \tag{28}$$

$$y_k = g(x_k,\ u_k) + v_k \tag{29}$$

As before, w_k and v_k are zero mean white Gaussian stochastic processes with covariance matrices $\sum v$ and $\sum w$, respectively. Now, f (.) is a nonlinear transition matrix function, and g (.) is a nonlinear measurement matrix.

At each time step, f (.) and g (.) are linearized by a Taylor-series expansion.

$$f(x_k, u_k) \approx f(\hat{x}_k, u_k) + \frac{\partial f(x_k,\ u_k)}{\partial x} \parallel_{\cdot x_k = \hat{x}_k} (x_k - \hat{x}_k) \tag{30}$$

$$g\ (x_k,\ u_k)\ \approx g(\hat{x}_k,\ u_k) + \frac{\partial g(x_k,\ u_k)}{\partial x} \parallel_{\cdot x_k = \hat{x}_k} (x_k - \hat{x}_k) \tag{31}$$

So, we have the linearized system:

State-space model:

$$x_{k+1} = f(x_k,\ u_k) + w_k \tag{32}$$

$$yk = gxy_k = g(x_k,\ u_k) + v_k, \qquad y_k = g(x_k, u_k) + v_k \tag{33}$$

where w_k and v_k are independent, zero-mean, Gaussian noise processes of covariance matrices $\sum v$ and $\sum w$, respectively.

Definitions:

$$A_k = \frac{\partial f(x_k, u_k)}{\partial x} \parallel x_k = \hat{x_k^{(+)}} \tag{34}$$

$$C_k = \frac{\partial g(x_k, u_k)}{\partial x} \parallel x_k = \hat{x_k^{(-)}} \tag{35}$$

Initialization: For k = 0, set

$$\hat{x_k^{(+)}} = E[x_0] \tag{36}$$

$$\sum\nolimits_{x_0}^{(+)} * = E[(x_0 - E[x_0])(x_0 - E[x_0])\Upsilon T] \tag{37}$$

Computation: For k = 1, 2, K, compute:

State estimate propagation:

$$\hat{x}_k^{(-)} = f\left(\hat{x}_{k-1}^{(+)},\ u_{k-1}\right) \tag{38}$$

Error covariance propagation:

$$\sum\nolimits_{e,k}^{(-)} * = A_k \sum\nolimits_{e,k-1}^{(+)} * A_k^T + \sum\nolimits_w \tag{39}$$

Kalman gain matrix:

$$L_k = \sum\nolimits_{e,k}^{(-)} * C_k^T \left[C_k \sum\nolimits_{e,k}^{(-)} * C_k^T + \sum v\right] [\![^{-1}] \tag{40}$$

State estimate update:

$$\hat{x}_k^{(+)} = \hat{x}_k^{(-)} + L_k \left[y_k - g\left(\hat{x}_k^{(-)}, u_k\right)\right] \tag{41}$$

Error covariance update:

$$\sum\nolimits_{e,k}^{(+)} * = (I - L_k C_k) \sum\nolimits_{e,k}^{(-)} * \tag{42}$$

$$x_{k+1} \approx\ A_k x_k + [f(\hat{x}_k,\ u_k) - A_k \hat{x}_k] + w_k \tag{43}$$

$$y_k \approx\ C_k x_k + [g(\hat{x}_k,\ u_k) - C_k \hat{x}_k] + v_k \tag{44}$$

Equations (32)–(44) give a summary of the extended Kalman filter from reference [27].

2.3.1. Electrochemical Model

The electrochemical model [29–31], reduced-order model [32–34], equivalent circuit model [35–37], and data-driven model [38,39] are the primary battery-electric models. By accurately representing battery concentration, electrode potential, and Butler–Volmer kinetics, the electrochemical model can simulate the complex interplay of chemical and electrical processes that occurs within the battery during intercalation. This enables better control and regulation of the battery's performance and lifespan [29]. The particle swarm optimization (PSO) method is then used to optimize important model parameters, resulting in the establishment of an electrochemical model to represent the electrochemical behaviors of batteries. The electrochemical model demonstrated strong prediction performance, although it required a large amount of computing during model simulation, as demonstrated by Sung and Shin [30]. Next, to integrate the electrochemical model into the BMS, a model implementation strategy was created. The primary benefit of employing an electrochemical model is the ability to acquire the reactions occurring within the battery. In real-time applications, it might be challenging to identify numerous characteristics, such as the compositions of the internal chemicals.

Furthermore, there are significant computing overheads associated with these electrochemical models, because they typically require the solution of several partial differential equations. Reduced-order electrochemical models can approximate full-order models with appropriate assumptions.

An estimated technique was developed with a way to capture and understand the diffusion of compositions inside batteries. This helps us to understand what is happening inside the battery [32]. Subsequently, a simplified electrochemical model based on physics was created to estimate the state of charge of lithium-ion batteries with Figure 8 showing a cross-sectional view of battery cells. To forecast the discharging capacity of the battery under different situations, a robust SOC estimation was accomplished using a battery with

a reduced-order model [34]. The simpler reduced-order models produced by this method have some information loss, but they are still preferable for real-time battery applications. Reduced-order models have significantly smaller computing overheads, and the measured current and voltage signals can be used to determine the corresponding parameters.

Continuum porous-electrode models use physics concepts to develop equations that explain all of the internal events that occur within a cell. These equations are linked by partial differential equations (PDEs). The models take into account many state variables that are vital for understanding what is going on inside the cell, incorporating the solid-state amount of lithium, $C_s(x,r,t)$; lithium present on the cell's surface, $C_s(x,t)$; the electrolyte's lithium content, $C_e(x,t)$; the solid's potential, ϕ_s(x,t); the electrolyte's potential, ϕ_e(x,t); and the lithium migration rate, j(x,t), between phases [40].

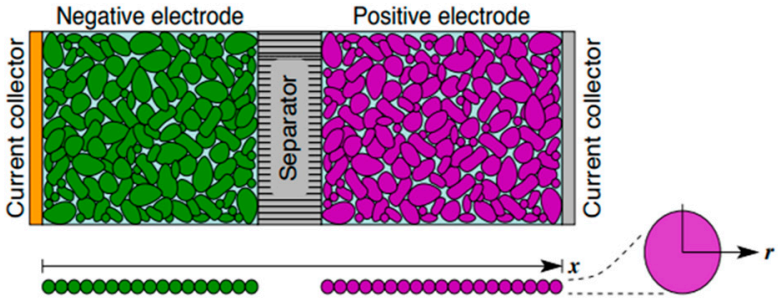

Figure 8. Typical battery cell cross-sectional view.

By resolving the five connected continuum-scale partial differential equations (as well as the corresponding boundary conditions), these five electrochemical variables can be determined.

Movement of Lithium-ions in the solid particles:

$$\frac{\partial C_s}{\partial t} = \frac{D_s}{r^2}\frac{\partial}{\partial r}\left(r^2\frac{\partial C_s}{\partial r}\right) \tag{45}$$

where C_s, D_s, and r are the concentration of lithium in the solid particles, diffusion coefficient in the solid, and radial coordinate within the particle, respectively. This equation represents Fick's law of diffusion in spherical coordinates.

Charge balance in particles; electron current:

$$\nabla.\left(\sigma_{eff}\,\nabla\phi_s\right) = a_s\,F\,j. \tag{46}$$

where ϕ_s, σ_{eff} , a_s, F, and j are the electric potential in the solid, effective conductivity of the solid, specific surface area of the particles, Faraday's constant, and reaction current density, respectively. This equation ensures that the divergence of the electric current in the solid balances the reaction current.

Diffusion of lithium in electrolyte:

$$\frac{\partial(\varepsilon_e C_e)}{\partial t} = \nabla.\left(D_{e,eff}\nabla C_e\right) + a_s\left(1 - t_+^0\right)j. \tag{47}$$

where C_e, ε_e, $D_{e,eff}$, and t_+^0 are the lithium concentration in the electrolyte, porosity of the electrolyte phase, effective diffusion coefficient co-efficient in the electrolyte, and transference number of lithium-ion, respectively. This equation accounts for the time-dependent change in lithium concentration in the electrolyte, considering both diffusion and reaction contributions.

Charge balance in electrolyte; ion current:

$$\nabla.\left(\kappa_{eff}\nabla\phi_e + \kappa_D\nabla\ln C_e\right) + a_s F j = 0. \quad (48)$$

The reaction rate (where $\eta = (\phi_s - \phi_e) - Uocp - j\ F\ Rfilm$) :

$$j = k_0 C_e^{1-\alpha}(C_{s,max} - C_{s,e})^{\ 1-\alpha} C_{s,e}^{\alpha}\left\{\exp\left(\frac{(1-\propto)F}{RT}\eta\right) - exp\left(-\frac{\alpha F}{RT}\eta\right)\right\} \quad (49)$$

It was discovered that these equations could be resolved using simulation; however, the method demanded a significant amount of processing power. Furthermore, past performance demonstrates that PDE simulators can be quite brittle, unable to converge to stable solutions.

A method to convert the PDEs into a discrete-time reduced-order model was suggested, and two fundamental presumptions in simulation were made [40]:

- The presumption was of linear behavior: a Taylor series was used to linearize the nonlinear equations.
- By assuming that the electrolyte concentration $C_e(x,t)$ was not a function of the reaction current j(x,t), transfer functions were built.

Next, a discrete-time state-space model was made using a technique known as the "discrete-time realization algorithm" (DRA), as shown below in Figure 9.

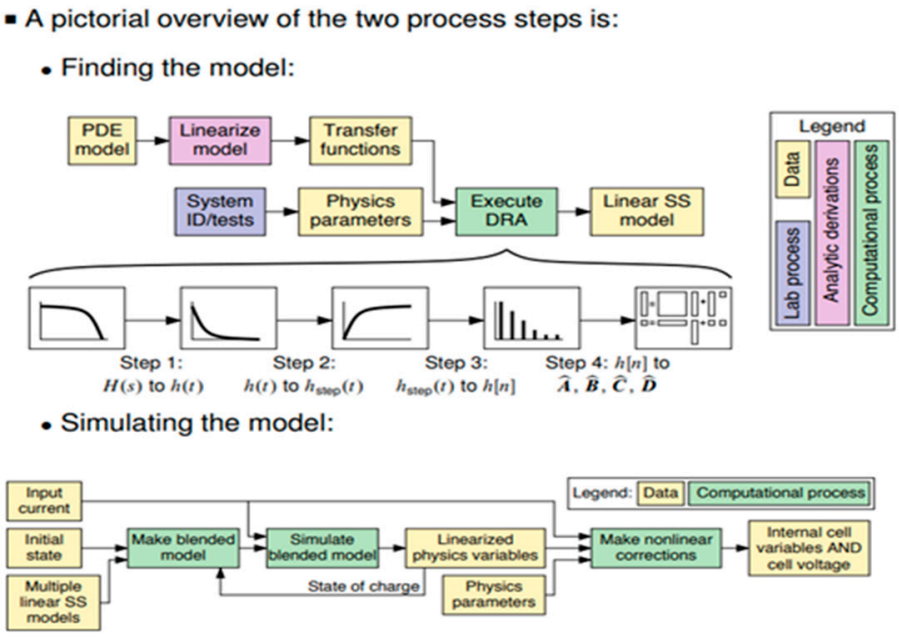

Figure 9. The DRA-produced ROM [40].

The challenges and limitations of electrochemical model (EM) methods in state of charge (SOC) estimation primarily revolve around their complexity and the need for detailed and accurate data. These models are computationally intensive due to their detailed representation of electrochemical processes. They require precise parameters that are sensitive to changes, such as battery aging, and these parameters can be difficult to obtain accurately. Additionally, EMs need extensive experimental data for calibration and validation, which can be time-consuming and costly. The effectiveness of EMs is highly dependent on the accuracy of the model in reflecting actual battery behaviors under various conditions, such as temperature fluctuations and aging effects. These factors collectively make EMs challenging to implement and maintain, especially for real-time applications.

2.3.2. Equivalent Circuit Model

The Partnership for a New Generation of Vehicles (PNGV) model, Rint model, Thevenin model, and the RC model are just a few of the analogous circuit models that are commonly used in EV research today [41,42].

- Rint Model

The Rint model defines the battery open-circuit voltage by implementing an ideal voltage source U_{OC}, as seen in Figure 10 and Equation (50). U_{OC}, which is the voltage when the circuit is opened, and resistance Ro are both influenced by temperature, SOC, and SOH. Terminal voltage (U_L) is equal to load current (I_L), which has a positive value when charging and a negative value when discharging.

$$U_L = U_{OC} - I_L R_0 \tag{50}$$

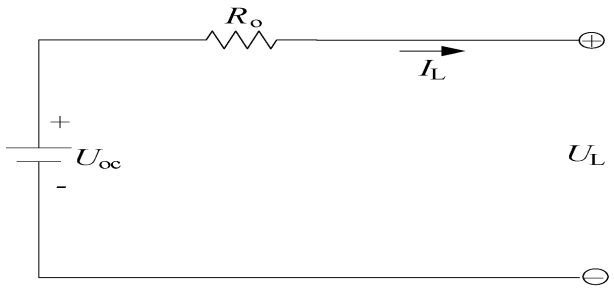

Figure 10. Schematic diagram of the Rint model.

- RC Model

$$\begin{bmatrix} \dot{U}_b \\ \dot{U}_c \end{bmatrix} = \begin{bmatrix} \frac{-1}{C_b(R_e+R_c)} & \frac{1}{C_b(R_e+R_c)} \\ \frac{1}{C_c(R_e+R_c)} & \frac{-1}{C_c(R_e+R_c)} \end{bmatrix} \begin{bmatrix} U_b \\ U_c \end{bmatrix} + \begin{bmatrix} \frac{-R_c}{C_b(R_e+R_c)} \\ \frac{-R_e}{C_c(R_e+R_c)} \end{bmatrix} [I_L] \tag{51}$$

$$[U_L] = \begin{bmatrix} \frac{R_c}{(R_e+R_c)} & \frac{R_e}{(R_e+R_c)} \end{bmatrix} \begin{bmatrix} U_b \\ U_c \end{bmatrix} + \left[-R_t - \frac{R_e R_c}{(R_e+R_c)} \right] [I_L] \tag{52}$$

This model is made up of three resistors (R_t, R_e, R_c) and two capacitors (C_c, C_b), as seen in Figure 11. The capacitor C_c, termed the surface capacitor, has a tiny capacitance and mostly depicts a battery's surface effects, while C_b is the bulk capacitor. A battery's ability to hold charge chemically is a result of its large capacitance, which is what bulk capacitors are known for. By measuring the voltage across the bulk capacitor, one can find the SOC. Terminal resistor, end resistor, and capacitor resistor are the names given to the resistors R_t, R_e, and R_c, respectively. The voltages across C_b and C_c are denoted by U_b and Uc, respectively. Equations (51) and (52) represent the electrical behavior of the RC model circuit.

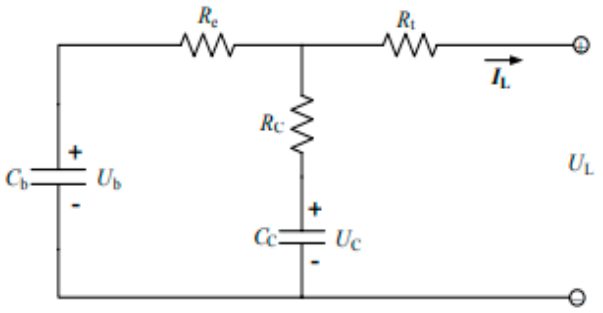

Figure 11. Schematic diagram of the RC model.

- The Thevenin Model

The Thevenin Model is primarily made up of three components, as seen in Figure 12: equivalent capacitances, internal resistances, and open-circuit voltage (U_{OC}). R_o and R_{Th} are examples of internal resistances. The transient response while charging and discharging is expressed in terms of the equivalent capacitance, or C_{Th}. C_{Th} voltages are represented by U_{Th}. The current that exits C_{Th} is denoted as I_{Th}. Equations (53) and (54) can be used to express the Thevenin model's electrical behavior.

$$\dot{U}_{Th} = -\frac{U_{Th}}{R_{Th}C_{Th}} + \frac{I_L}{C_{Th}} \tag{53}$$

$$U_L = U_{OC} - U_{Th} - I_L R_O \tag{54}$$

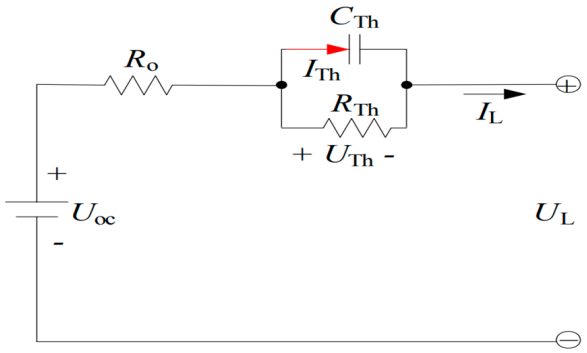

Figure 12. Schematic diagram of the Thevenin model.

- The PNGV Model

Figure 13 illustrates a PNGV model with an open-circuit voltage source U_{oc}, in series with an internal resistance R_o and a dynamic element represented by a capacitor $1/U'_{oc}$ and a voltage U_d; alongside this series connection is a parallel network of a capacitor C_{PN} and resistor R_{PN}, with the current I_{PN} flowing out of C_{PN}, and the entire assembly is connected to a load characterized by a current I_L and voltage U_L, forming a modified Thevenin equivalent circuit that models the variable open-circuit voltage behavior under load conditions. The electrical behavior of the PNGV model can be expressed by Equation (56):

$$\dot{U}_d = \dot{U}'_{OC}\, I_L \tag{55}$$

$$\dot{U}_{PN} = \frac{U_{PN}}{R_{PN}C_{PN}} + \frac{I_L}{C_{PN}} \tag{56}$$

$$U_L = U_{OC} - U_d - U_{PN} - I_L R_0 \tag{57}$$

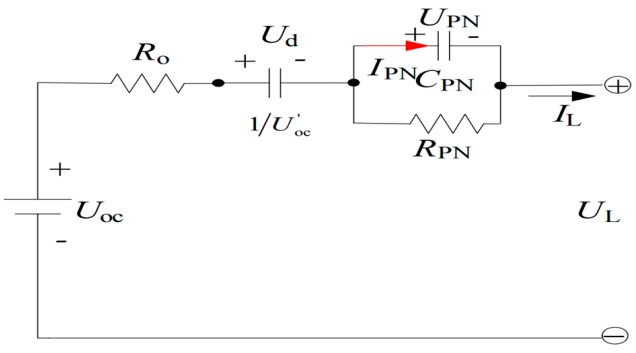

Figure 13. PNGV model.

- The Dual Polarization (DP) Framework

The test framework shows that polarization is one of a lithium-ion battery's properties. The Thevenin model might replicate the polarization characteristic to some extent, but in the final moments of charge or discharge, the differences between concentration polarization and electrochemical polarization result in an erroneous projection. To more accurately describe polarization features and simulate concentration and electrochemical polarization independently, an enhanced circuit model, referred to as the dual polarization (DP) model, is shown in Figure 14.

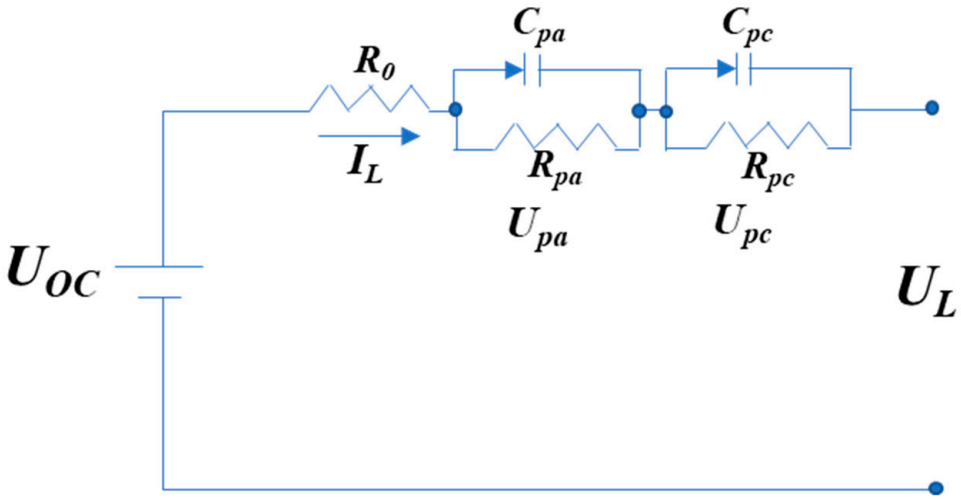

Figure 14. Schematic diagram of the dual polarization model.

The DP model is divided into three sections: The first three parameters are the OCV (U_{oc}); the second is the internal resistance, which includes the ohmic resistance Ro and the effective resistances R_{pa} and R_{pc}, which characterize the electrochemical and concentration polarization, respectively; and the third is the effective capacitance, which includes C_{pa} and C_{pc}, which describe the concentration and electrochemical polarization separately and characterize the transient response during power transfer to and from the battery. U_{pa} and U_{pc} represent C_{pa} and C_{pc} voltages, respectively. The currents of C_{pa} and C_{pc} are I_{pa} and I_{pc}, respectively. Equation (60) can be used to express the circuit's electrical behavior:

$$\dot{U_{pa}} = -\frac{U_{pa}}{R_{pa}C_{pa}} + \frac{I_L}{C_{pa}} \tag{58}$$

$$\dot{U_{PC}} = \frac{U_{pc}}{R_{pc}C_{pc}} + \frac{I_L}{C_{pc}} \tag{59}$$

$$U_L = U_{oc} - U_{pa} - U_{pc} - I_L R_0 \tag{60}$$

2.3.3. Electrochemical Impedance Model

In addition to incorporated components and porous electrode theory, the electrochemical impedance model (EIM)-based SOC assessment incorporates additional parameters into the model by including Warburg, constant phase, and Z_{arc} elements [43–46]. A basic schematic diagram of the EIM is displayed in Figure 15. A potent method for examining the internal dynamics of batteries across a variety of periods is electrochemical impedance spectroscopy (EIS). The electrochemical system comprising the battery's capacitive and inductive components may be recognized and measured by EIS by measuring the battery's impedance throughout a broad frequency range [47]. Electric double-layer effects, ion diffusion, and charge transfer reactions are just a few of the internal processes that may be

understood by estimating the battery's impedance using these measures. Battery research and diagnostics have found that EIS is a useful tool, as it produces accurate findings with little computing demand when combined with an appropriate electrochemical model, such as the EIM.

The EIM method, used in SOC estimation, encounters several specific limitations. Firstly, EIM is inherently complex in its interpretation, as it relies on analyzing impedance spectra. This complexity necessitates specialized knowledge, making EIM less accessible for standard applications. Moreover, the method's accuracy is highly sensitive to operational conditions like temperature and battery aging. Fluctuations in these factors can lead to significant variances in impedance response, thereby affecting the precision of SOC estimations.

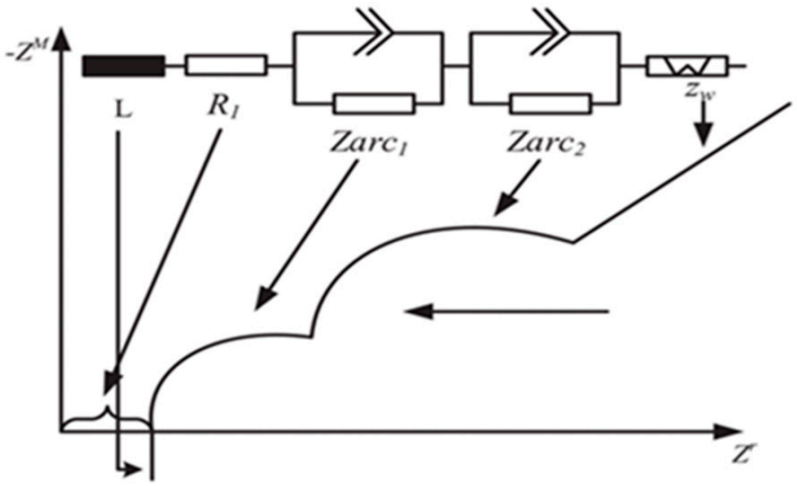

Figure 15. Schematic diagram of EIM.

In addition, EIM demands a comprehensive understanding of the battery's electrochemical properties, involving detailed and complex electrochemical analysis. This requirement often makes EIM a more specialized approach, limited to scenarios where such expertise is available. Another considerable limitation is the time-intensive nature of impedance spectroscopy measurements. These measurements often require the battery to be in a stable state, which limits the method's applicability in dynamic or real-time scenarios, where quick and responsive SOC estimation is crucial.

Furthermore, EIM requires specialized and often costly equipment to measure impedance spectra, which may not be practical or affordable for all applications. The method's effectiveness also varies across different types of batteries, and it may not be suitable for all battery chemistries or designs. Lastly, translating impedance data into accurate SOC values involves complex modeling, especially challenging due to the nonlinear behavior of batteries.

In summary, while EIM offers detailed insights into a battery's electrochemical processes, its practical application in SOC estimation is constrained by its interpretational complexity, operational sensitivity, specialized knowledge requirements, measurement constraints, equipment costs, battery type limitations, and the complex modeling needed for accurate data translation.

If the battery is accurately modeled, precision is the benefit of model-based SOC estimation. This has been demonstrated in [48], where EIM and EKF are combined to assess SOC for lithium batteries. Additionally, according to some researchers, model-based SOC estimation produces strong closed-loop control, high adaptability, and good real-time performance [49]. Unfortunately, based on models, modeling complexity is a drawback of the

accurate SOC prediction approach. Considering the great variation in battery chemistries and constructions, this might be a significant obstacle to researchers in fully comprehending the distinctive electrochemical characteristics of the particular battery type they are modeling [50]. The exhaustive experimentation necessary to determine the correlations between numerous factors adds to the process's time-consuming nature [51]. The difficult work of identifying every important parameter that goes into creating a strong model frequently requires iterative testing and improvement. Sometimes, an extra Warburg element—which symbolizes the battery's frequency-dependent diffusion impedance—is added to these models to improve their accuracy for specific batteries. This adds another level of complexity, but improves the model's ability to mirror actual battery behavior [52]. Creating an excellent model is usually difficult and necessitates extensive prior knowledge. Consequently, it is not always feasible to apply the model-based approach to all battery types.

2.4. Data-Driven Model Estimation

Battery parameters like current, voltage, and temperature can be measured and used in data-based techniques for SOC estimation. As a result, an additional filter in the model-based approach is avoided [53]. Additionally, the self-learning algorithm determines the network parameters of data-driven methods [54]. This process is entirely different from model-based estimation techniques, which require significant time and human expertise for parameter estimation.

Machine learning (ML) platforms are frequently required in data-driven approaches to extract relationships and rules from the data [55]. Their algorithms are used today to achieve on-par or sometimes even super-human performance in a variety of fields, including medical diagnosis [56], stock trading [57], robotics [58], mastering board games [59], and more.

This section concerns data-driven approaches for battery SOC estimation.

2.4.1. Neural Network Method

A neural network (NN) is a created intelligence that learns from examples and improves with time. Consider it similar to training a machine to spot patterns. In this example, it is utilized to anticipate how much charge a battery has remaining.

There are two major steps. First, it follows through with a calculation process step by step, much like adding numbers. It then double-checks its replies and corrects any errors. It makes use of battery performance metrics, such as how much power the battery is using, the temperature, and the battery resistance, as input data [59–61]. Depending on all of these variables, our neural network assists us in determining a battery's level of charge. The hidden layer serves as the system's activation function. Figure 16 depicts the basic processing sequence of a neural network method. The experimental results validate the resilience and accuracy of this technique, which provides a quick and efficient calculation of SOC.

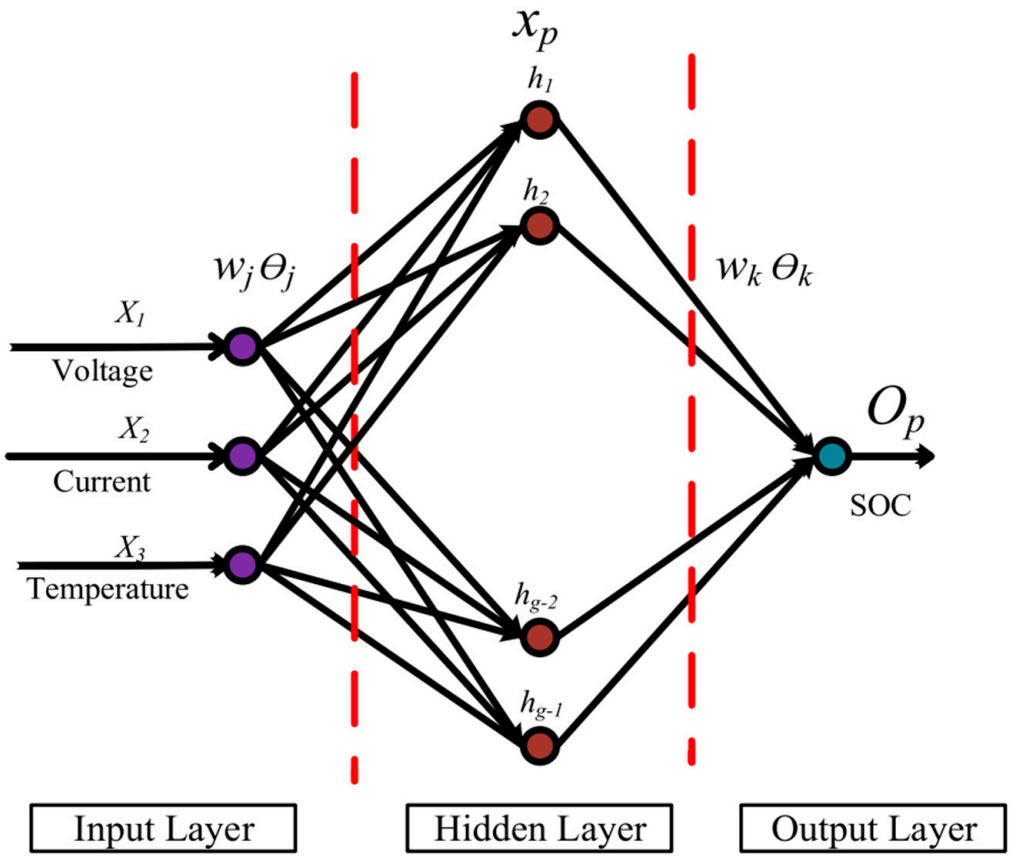

Figure 16. Three-layer neural network architecture for SOC estimation [62].

Despite its benefits, this strategy has inherent limits. A large number of training data are used to adequately train the algorithm. The quantity and quality of training data have a considerable influence on accuracy [63,64]. In summary, NNs for SOC estimation face drawbacks such as a heavy reliance on extensive data for training, risk of overfitting, opaque 'black box' decision-making processes, computational intensity in training, sensitivity to network architecture and hyperparameters, challenges in generalizing across different battery types, reduced adaptability in non-stationary environments due to battery aging or usage pattern changes, and the requirement for specialized machine learning expertise for development and tuning.

The use of deep learning (DL) algorithms in the state estimation of BMS is made feasible by the advancement of big data and cloud computing platforms. The term "deep" is used by the so-called DL algorithms to characterize the utilization of several hidden layers or other distinct architectural styles [65]. Deep learning algorithms can map complex and nonlinear functions more accurately and effectively than shallow neural networks. This research categorizes standard DL algorithms into three groups based on their architectures: convolutional neural network (CNN), recurrent neural network (RNN), and deep neural network (DNN). The fundamental ideas and uses of these three SOC estimating techniques are thoroughly described in this section.

- Deep Neural Network

A deep neural network (DNN) is an extension of a back-propagation neural network (BPNN) with additional hidden layers, as shown in Figure 17. Each hidden layer may contain a different number of hidden neurons, represented by l_1, … l_M. Both DNN and BPNN use the same learning method and information transformation principles. A multilayer feed-forward NN was developed to tackle the common issues of over-fitting or underfitting in data-driven approaches for SOC estimation [66]. The NN was built from scratch,

starting with a basic version that had a low-dimensional input vector and gradually working its way up to a more complex structure with a high-dimensional input vector.

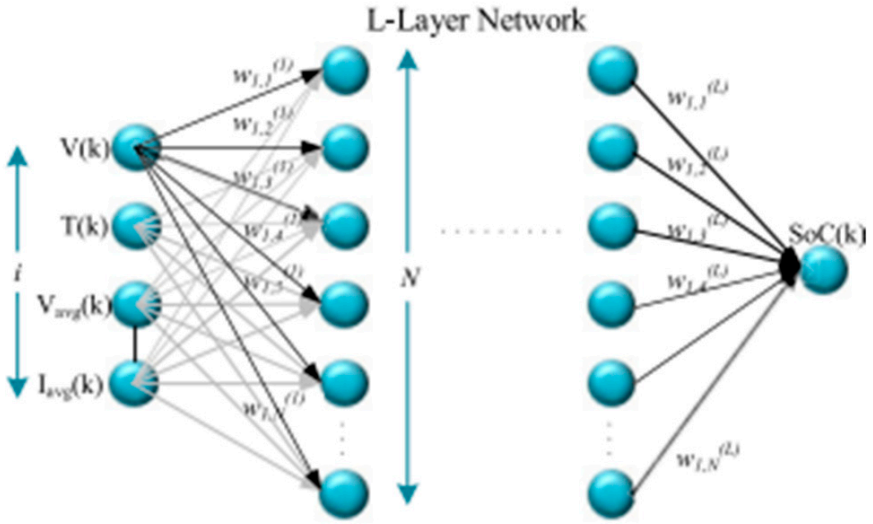

Figure 17. Deep learning network architecture for SOC estimation [53].

Although this constructive strategy was largely a trial-and-error approach, it is a crucial stage in the training of DNNs. An additional innovation was the use of the unscented Kalman filter (UKF) to filter the DNN outputs, which helped to increase their accuracy. After noise reduction, the suggested method's root mean square error (RMSE) was 1.4%, and its maximum error was only 1.9%, which is less than 2% under the Federal Urban Driving Schedule (FUDS) driving cycles. However, it is worth noting that the execution time of the algorithm could be significantly increased by merging UKF. A four-hidden-layer DNN with 64 neurons per hidden layer was found to be the best model after comparing numerous DNN models [53]. The number of hidden neurons and the number of hidden layers are important for accuracy and computing load.

DNNs encounter several drawbacks, including a substantial need for large datasets for training, high susceptibility to overfitting, considerable computational resources for model training and operation, complexity in architecture leading to difficulties in tuning and optimization, a "black box" nature that obscures interpretability of the decision-making process, and potential challenges in generalizing to new or unseen data, especially when operational conditions significantly deviate from the training scenarios.

- Convolutional Neural Network

CNN is used in lithium battery state estimation research. A typical CNN includes convolutional and pooling layers, fully connected layers, and an output layer, as shown in Figure 18. In CNN, neurons in each convolution layer are not connected to every other neuron, unlike in a fully connected network. This is achieved by sliding a filter across the input space, resulting in sparse connectivity. Convolution is a process where subsets of input space multiply with a filter. Three factors determine this process: filter size, number of filters, and step. This process allows for faster learning and reduced memory usage. Pooling layers decrease the size of feature maps. Rectified linear unit (ReLU) activation is typically used in a CNN.

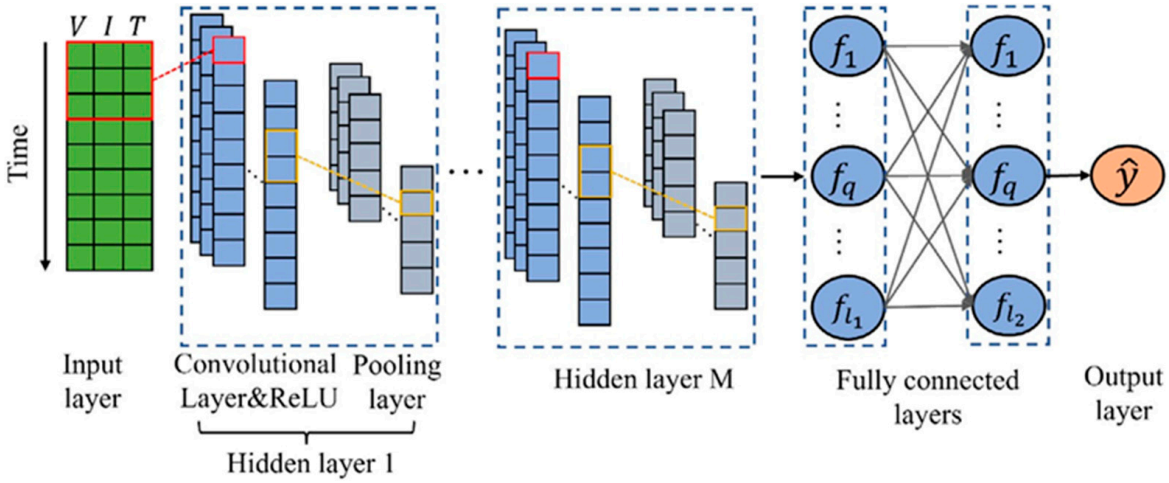

Figure 18. The structure of CNN [67].

Hybrid CNN–RNN networks are often used to estimate SOC. In one study, a CNN–long short-term memory (LSTM) network was used to capture spatial features and retrieve characteristics [68]. Different research conducted suggested the utilization of a CNN–gated recurrent unit (GRU) network; however, it deviated from employing average current and voltage as input parameters [69]. This hybrid network solely applied the one-dimensional convolution layer to extract relevant information from temperature, current, and voltage measurements. Hyperparameters were selected by comparing various designs. The suggested hybrid network was compared to other machine learning algorithms under driving cycles to confirm its superiority.

SOC can now be estimated using a 1D CNN alone for electric vehicles' batteries. The proposed model predicts SOC at timestep k using voltage, current, and temperature data from $k - t_w + 1$ to k as inputs. This model outperformed other techniques in terms of both performance and offline training time. Hannan et al. [70] proposed a fully convolutional network (FCN) with temporal convolutions for determining the state of charge. They used global average pooling to prevent overfitting. The model's learning rate was optimized using various techniques to better its error rate. The model achieved an MAE of 0.7% at room temperature and also an RMSE of 0.85%

CNNs encounter drawbacks such as their substantial need for large and diverse training datasets, vulnerability to overfitting, particularly when training data are limited, high computational requirements for training and inference, and the complexity of model architecture, which necessitates fine-tuning and specialized expertise to optimize effectively.

- Recurrent Neural Network

RNNs and BPNNs share some structural similarities, with RNNs evolving from feed-forward neural networks. This segment reviews RNN principles and their recent applications in SOC estimation.

Nonlinear autoregression with exogenous input neural network (NARXNN) is a neural network used for predicting one-time series. It uses historical values, feedback, and an external time series for training. Its layout is shown in Figure 19. It is a variation of the Jordan NN with a feedback mechanism. The expression of NARXNN is as follows:

$$y(n) = f_0\left[b_0 + \sum_{h=1}^{l} w_{h0} f_h\left(b_h + \sum_{i=0}^{d_u} w_{ih} x(n-i) + \sum_{j=0}^{d_y} w_{jh} y(n-j)\right)\right] \quad (61)$$

where h and l are the number of hidden neurons; $f_o(\cdot)$ and $f_h(\cdot)$ are activation functions of the output layer and hidden layer, respectively; d_u and d_y represent the input and output delays, respectively; and $[b_h, b_o]$ and $[w_{ih}, w_{jh}, w_{ho}]$ are biases and weights between the corresponding layers, respectively.

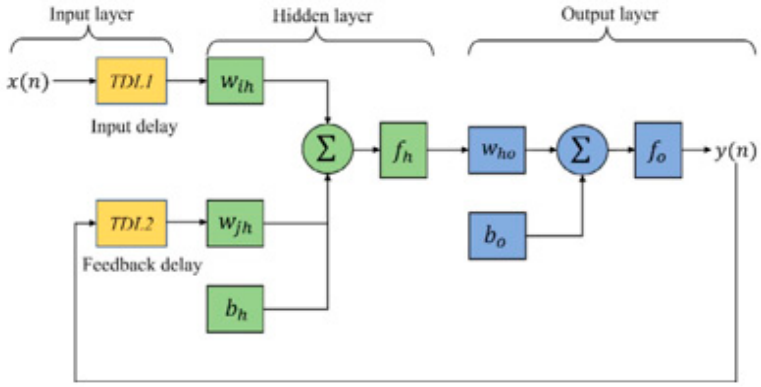

Figure 19. The structure of the NARXNN [71].

Time-sequence knowledge is enhanced by the prior knowledge of inputs and outputs. This is especially useful for SOC estimates and has generated much attention in this field. For SOC estimation, a dynamic neural network model based on the NARX structure was proposed [72]. An actual dataset of driving cycles of an electric vehicle, obtained from 54 different 800 km trips with varying unknown initial SOCs, was used. In all scenarios, the proposed approach is capable of producing accurate results. Particle swarm optimization (PSO) and latent semantic analysis (LSA) optimization techniques were found to improve NARXNN's SOC estimation capabilities in a study [73]. Heuristic optimization methods can be used to save time and allow for model performance tweaking. NARXNN alone, as a result of noises, can lead to noisy estimation [74]. To enhance the overall SOC estimation method's robustness, adaptability, and efficiency, Qin et al. [75] combined the NARXNN and UKF algorithms, similar to [71]. RNNs often experience gradient fading issues, which in this case were solved using a moving window approach based on the conventional finite-element concept [76]. The enhanced NARXNN adjusts historical data by changing the window size at the right moment, avoiding gradient issues, and increasing estimation accuracy.

RNNs, when used for applications like SOC estimation, encounter specific drawbacks including a tendency to fade, significant computational resources required for training and operation, and challenges in model tuning and hyperparameter optimization, all of which require substantial machine learning expertise to address effectively.

2.4.2. Deep Learning

Vapnik introduced support vector machines (SVMs), another well-liked and often-used machine learning algorithm that may be utilized for both regression and classification issues, particularly with smaller datasets [77]. Originally designed to address classification issues, SVMs were later extended to address regression issues and given the name support vector regression (SVR) [78]. In general, a large number of regression issues are not amenable to linear regression in the input space.

As a result, one of SVM's benefits is to permit linear separation. The basic tenets of SVM theory can be found in references [77,78].

Let us choose a training dataset $\mathfrak{D} = \{(\boldsymbol{x}_i, y_i)\ , i = 1, \ldots, L\}$ where $\boldsymbol{x}_\mathrm{i}$ and $\mathrm{y_i}$ represent the input and output vector, respectively; the support vector machine is defined as:

$$f(\boldsymbol{x}_i) = W^T.\,\phi(\boldsymbol{x}_i) + b,\ \boldsymbol{w} \in \mathbb{R}^{\boldsymbol{n}}, \boldsymbol{x_i} \in \mathbb{R}^{\boldsymbol{m}}, \boldsymbol{b} \in \mathbb{R} \tag{62}$$

where b and W are the parameters to be determined; φ(·) is a mapping function; and $(\mathbb{R}^m)$ and $(\mathbb{R}^n)$ are the input and high-dimensional space, respectively. The input data can be linearly segregated in the new feature space. The SVM model employs more advanced methods to compute the ϵ-insensitive loss function, in contrast to basic linear regression models. Slack variables ξ_i^+ and ξ_i^- are added to the hard margin to produce a so-called soft margin, as seen in Figure 20, to make the optimization possible.

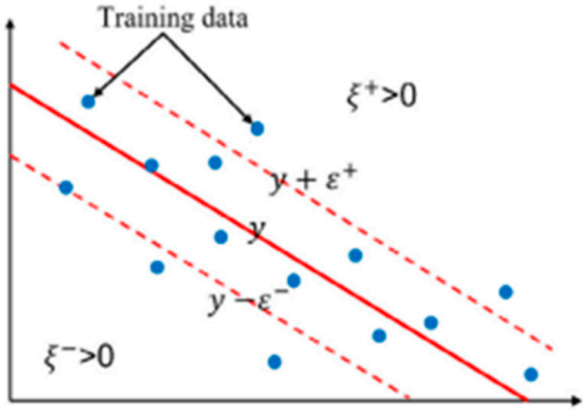

Figure 20. Illustration of the SVM.

Numerous researchers have used support vector machines (SVMs) for SOC estimation due to their strong regression capabilities with tiny sample sizes. An SVM-based approach has been used to calculate SOC utilizing temperature, voltage, and current information gathered from working cycles at various DST driving cycles [79]. In addition to validating the SOC prediction's performance, this approach was utilized to determine the ideal hyperparameters. The findings show that throughout the whole test, the RMSE was just 0.71%, and the prediction errors were consistent within 6% in each case. Various tactics were employed [71,80] to train and identify the ideal parameters, enhancing model performance. To cut down on the amount of time needed to search for optimal pairs of hyperparameters, Hu et al. [71] employed a double-step search strategy. The particle swarm optimization algorithm was used to determine the hyperparameters of the SVM model, namely the RBF's kernel width (σ) and penalty factor (γ). The particle swarm optimization model demonstrated the benefits of increased estimation accuracy and quicker processing performance when compared to the SVM model using a standard approach. Furthermore, the suggested method's generalizability was confirmed under four lithium-ion battery fault states: excessive internal resistance, excess temperature, and terminal voltage above the upper or lower cut-off voltage. Under these four battery failure scenarios, the suggested method's average errors were all less than 2.5%.

The primary drawback of using an SVM for SOC estimation is its sensitivity to the choice of kernel and hyperparameters, which requires careful tuning, along with its potential difficulty in handling large datasets due to computational complexity, and limited interpretability of the model's decision-making process.

2.4.3. Fuzzy Logic

A computational method that provides flexibility in a statement is called fuzzy logic (FL). This method makes it easier to understand the idea of partial truth, in which the truth

value might be, depending on a number between 0 and 1, entirely true, partially true, or fully false [81]. FL presents the idea of many-valued logic as an alternative to the traditional two-valued true-or-false logic. Fuzzification, fuzzy rule base, inference engine, and defuzzification are used in the framework of the FL interface system [82]. A few studies using FL to estimate SOC are available. FL and SVM can be used to suggest the SOC of a battery pack in an electric vehicle [83].

In comparison to NN and standard SVR, the authors found improvements in SOC estimate accuracy and noise immunity. A strong-tracking adaptive unscented Kalman filter (ST-AUKF) technique was developed to estimate SOC. It is based on a dynamic parameter that varies according to conditions or inputs, allowing the control algorithm to adjust the influence of past data, either giving more weight to recent data or considering historical data, depending on the system's changing circumstances and uncertainties [84].

The fuzzy adaptive forgetting factor is critical in updating the battery model parameters, which ensures that the model adapts to changing situations and retains accurate representations of the battery's behavior over time. Compared to the traditional UKF technique, the suggested model may yield better results in terms of accuracy, robustness, and convergence time. A fuzzy-logic-based SOC estimate model was developed by Singh et al. [85] through the analysis of voltage and impedance data. Using fuzzy logic and data from impedance spectroscopy, Salkind et al. [82] calculated SOC. The designed model is implemented using an analog-to-digital converter, temperature sensor, current sensor, and Motorola 68HC11 microprocessor (LM35CZ). The error range is constrained to less than 5%, and the hardware is checked using LIBs.

The enhanced approach known as the adaptive neuro-fuzzy inference system (ANFIS) combines the fuzzy inference system with the NN learning method without requiring a detailed battery model. In terms of modeling, decision-making, and signal processing, ANFIS is incredibly potent [86,87].

Using inputs such as current, temperature, cooling air temperature, and battery thermal factor, an ANFIS-based SOC estimate model can be constructed. Ten distinct driving cycles are used to assess the training and testing outcomes.

The findings show that in varied driving cycles, the ANFIS model performs with an SOC error of less than 1%. To calculate SOC for lithium-ion batteries, an ANFIS model was constructed in [88] using current, voltage, capacity, and temperature. It is stated that the average percentage inaccuracy is merely 0.53%. Figure 21 shows the ANFIS structure with five computations for its SOC estimation. The five-stage ANFIS configuration's mathematical representations are given in Equations (63)–(70).

$$\mu_A = \frac{1}{1 + \left|\frac{x - c_i}{a_i}\right| 2b_i} \tag{63}$$

$$\{Q_{2,1} = w_1 = \mu_{A2}(x)\,\mu B_1(y) \tag{64}$$

$$\{Q_{2,2} = w_2 = \mu_{A2}(x)\,\mu B_2(y) \tag{65}$$

$$Q_{3,1} = \overline{w}_1 = \frac{w_1}{w_1 + w_2} \tag{66}$$

$$Q_{3,2} = \overline{w}_2 = \frac{w_2}{w_1 + w_2} \tag{67}$$

$$Q_{4,1} = \overline{w}_1 f_1 = \overline{w}_1 (p_1 x_1 + q_1 y_1 + r_1) \tag{68}$$

$$Q_{4,2} = \overline{w}_2 f_2 = \overline{w}_2 (p_2 x_2 + q_2 y_2 + r_2) \tag{69}$$

$$Q_5 = \sum_{i=1}^{2} \overline{w}_i f_i = \frac{\sum_{i=1}^{2} \overline{w}_i f_i}{\sum_{i=1}^{2} \overline{w}_i} \tag{70}$$

The drawbacks of using fuzzy logic for SOC estimation include its reliance on expert knowledge for rule formation, potential challenges in precisely defining membership functions, limitations in handling complex systems with high-dimensional data, the subjective nature of rule-based systems leading to possible inconsistencies, and difficulties in integrating with other numerical methods due to its qualitative approach.

The table below highlights the components of the ML algorithms used for SOC estimations examined in the previous section: input and output characteristics, performance metrics, a portion of the suggested algorithms' hyperparameters, and the data profiles used to train and verify the models. Furthermore, Table 1 provides a summary of genetic algorithm (GA) and fuzzy logic (FL).

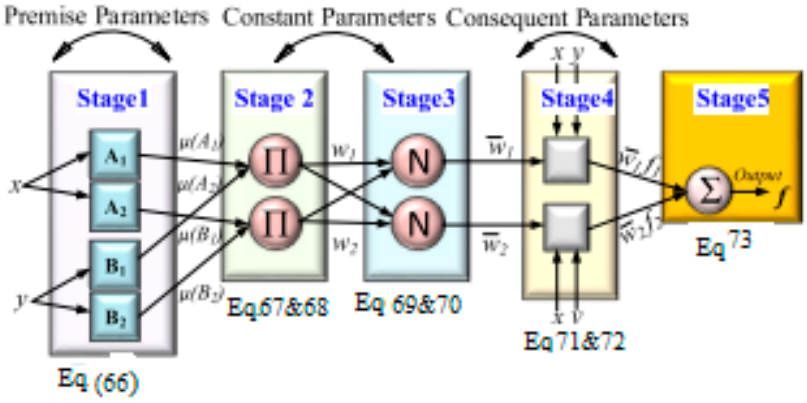

Figure 21. ANFIS structure for SOC estimation [88].

Table 1. Machine learning algorithm SOC methods.

Algorithm	Input	Output	Metric	Hyperparameter	Data Profile
Linear Regression (LR)	Voltage, Current, Temperature	SOC	RMSE Root Mean Squared Error, MSE Mean Squared Error MAE Mean Absolute Error	Learning Rate (LR), Regularization (REG)	Cycles, Temperature Variant
Support Vector Machine (SVM)	Voltage, Current, Temperature	SOC	Accuracy, Precision, Recall	Kernel, C, Gamma (γ)	Cycles, Load prof
Back-Propagation Neural Network (BPNN)	Voltage, Current, Temperature	SOC	Coefficient of Determination R^2, MSE, RMSE	LR, Momentum (MOM), Layers	Lab, Driving past
Recurrent Neural Network (RNN)	Voltage, Current, Temperature	SOC	Accuracy, RMSE, MAE	RNN Layers, Cells	Seq data, Temp Corr
Adaptive Neuro-Fuzzy Inference System (ANSFIS)	Voltage, Current, Temperature	SOC	Rule Accuracy, RMSE	Rules, Membership Functions (MFs)	Expert knows, Fuzzy rules
Nonlinear Autoregressive with Exogenous Input Neural Network (NARXNN)	Voltage, Current, Temperature	SOC	R^2, MSE, Accuracy	Delays, Neurons	Series, Feedback loops

Table 1. *Cont.*

Algorithm	Input	Output	Metric	Hyperparameter	Data Profile
Genetic Algorithm (GA)	Voltage, Current, Temperature	SOC	Conversion Rate, Accuracy	Population Size (POP Size), Mutation Rate (Mut), Crossover Rate (Xover)	Param opt, Feature sel
Fuzzy Logic (FL)	Voltage, Current, Temperature	SOC	Rule Accuracy, Interpretability	MFs, Rule Base	Expert knows, Op data
Long Short-Term Memory (LSTM)	Voltage, Current, Temperature	SOC	Accuracy, RMSE, MAE	LR, Units, Dropout	Series, Charge/discharge
Gradient Boosting Machines (GBM)	Voltage, Current, Temperature	SOC	MAE, RMSE, R^2	LR, Estimators, Depth	Cycles, Aging data
Random Forest (RF)	Voltage, Current, Temperature	SOC	R^2, MSE, RMSE	Trees, Depth, Split	Lab, Real-world use
Reinforcement Learning	Voltage, Current, Temperature	SOC	Reward, Error Rate	Learning Rate, Discount Factor	Simulated environments
PCA + ML Model	Voltage, Current, Temperature	SOC	R^2, MSE, RMSE	Components, ML Hyperparameters	Noise-reduced data
Ensemble Methods	Voltage, Current, Temperature	SOC	Accuracy, RMSE, R^2	Number of Models, Strategy	Diverse driving patterns
Deep Belief Networks	Voltage, Current, Temperature	SOC	R^2, MSE, MAE	Layers, LR, Epochs	Multivariate time series
Convolutional NN	Voltage, Current, Temperature	SOC	Accuracy, Precision, Recall	Filters, Kernel Size	Image, Sequential data
k-NN	Voltage, Current, Temperature	SOC	Accuracy, RMSE, Precision	Number of Neighbors	Cycles, Driving conditions
Decision Trees	Voltage, Current, Temperature	SOC	Accuracy, R^2, RMSE	Depth, Min Samples	Cycles, Varied temps

3. SOH Estimation

Battery SOH is a performance metric that compares a battery's current capacity with respect to its full original capacity (as a fresh battery) and is expressed as a percentage. It is a good indication of a battery's current condition and future life expectancy. Aging causes a decrease in battery capacity and an increase in internal resistance for EV applications; the factors are represented in Equation (71):

$$\int_{\tau=t_0}^{t} \delta_{func}(I,\ T,\ SOC,\ others)d\tau \tag{71}$$

δ_{func} is an aging rate function that quantifies how quickly or slowly the battery degrades or ages over time. Therefore, internal resistance can help in the estimation of SOC [89]. There are three types of methods that have been proposed to estimate battery SOH: data mining, model-free, and model-based methods.

Battery SOH can be simply defined as:

$$\begin{cases} SOH = C_{aged}/C_n \times 100\% \\ SOH = R_{inc}/R_n \times 100\% \end{cases} \tag{72}$$

where C_n and R_n stand for the nominal capacity and internal resistance, respectively, of the new battery without being used, C_{aged} for the aged capacity, and R_{inc} for the internal impedance.

Equation (72) defines SOH as follows: the aged capacity and internal impedance of a battery are measured using the pulse current test [90] or the standard capacity test [91]. Since a full discharge using regulated current and temperature will disrupt regular EV operations, this direct method is awkward and not advised. Electrochemical impedance spectroscopy (EIS) of batteries can undoubtedly provide a great deal of information about their state of health compared to the direct measurements of internal impedance and the aged capacity. Therefore, the electrochemical impedance spectroscopy of batteries was suggested by researchers for use in health diagnosis [92,93]. Its applicability is limited due to the uniqueness of instruments that are required for the measurement and application of battery electrochemical spectroscopy. Furthermore, it takes a long time to complete an EIS test.

In the model-based approach, the electrochemical model [94] and the battery equivalent circuit model [95] are used to determine the time-varying parameters, such as battery capacity or internal resistance. The resistance during battery operations is then estimated using a variety of observers, including particle filters [96], Kalman filters [97], and sliding mode [98], allowing the SOH to be determined appropriately. However, the decay in the battery capacity is defined as:

$$C_{decay} = \left(C_{aged} - C_n\right)/C_n \times 100\% \tag{73}$$

such that,

$$C_{decay} = \delta_{func}(f)Ah^z \tag{74}$$

f represents the stress factors, which are external factors or conditions that contribute to the degradation of a system, z is a parameter used to model how the capacity of the system decreases as a function of the cumulative current passing through it, and δ_{func} represents the aging rate function.

Numerous studies are consulted for the dynamics of battery aging, because battery capacity degradation is influenced by the temperature, current, SOC, and charging techniques of the battery, among other factors. Wang et al. created a model that predicts how long a battery would survive after repeated charging and discharging cycles using a mathematical equation known as the power law [99]. With no regard for the depth of discharge, the battery model was calibrated across broad SOC parameter ranges such that a cycle-life model at constant temperature was used to forecast a capacity loss in batteries at low SOC levels [100]. A battery aging model was used to forecast lower capacity under both fast charging and discharging conditions [101]. To capture the dynamics of capacity deterioration under changing load circumstances, a cycle-life and dynamic cycle-life model based on a mechanistic and prognostic model were also presented [102,103]. According to Gao et al.'s analysis [104] of battery aging under various charging circumstances, active material loss is impacted by charging currents less than 1 C and cut-off voltages less than 4.2 V. To maximize real-time operations and extend battery service life, these cycle-life models are crucial. However, the majority of research being done now is focused on particular workloads. In real-time applications, there is no guarantee of their accuracy. More test data and a larger range of battery operations are used in training the battery model, which naturally increases its practical implementation due to SOH being more dynamic than SOC.

Data mining techniques have been used for battery SOH estimation, such as battery SOC estimation [105–107]. Klass et al. employed support vector machine (SVM) to determine the condition of a battery. It is similar to a diagnostic tool in that it tells us how well a battery is performing and whether or not it is still in excellent condition [108]. To generate the input and output vectors of the necessary SVM training dataset, a new data processing technique is proposed that makes use of load collectives. For battery capacity estimation, Hu et al. [106] used the K-nearest neighbor (KNN) method, a data-driven classification technique. Neural network and clustering are techniques used to estimate the battery SOH based on the historical distributions of the temperature, current, and voltage of the battery [109].

The estimation error of the SOH is seen to be within 2.15% in an average practical setting.

3.1. Review of ML SOH Estimation Algorithm

A certain amount of capacity- or resistance-based estimation can be used for SOH estimation. SOH is difficult to measure with commonly used sensors, much like the SOC of LiBs. This makes it a difficult assignment for BMS. We concentrate on ML techniques for SOH estimation in this section.

A reliable and accurate estimate of SOH cannot be guaranteed by the raw data, because they do not contain enough information to reflect SOH directly. Consequently, the second stage involves removing related features from sourced data using several methods, including differential voltage analysis (DVA) and model-based techniques. The degradation modes and aging mechanisms of the battery must be examined, and a connection with the health features must be made, before selecting any health characteristics. Then, correlation analysis is applied.

This section mainly reviews different ML algorithm applications for SOH.

3.1.1. Shallow Neural Network

The nonlinear relationship that exists between inputs and outputs can be mapped by the back-propagation neural network (BPNN) and radial basic function neural networks (RBFNN). Thus, SOH estimation has frequently employed these two types of NNs. To take a more realistic approach to the surroundings of electric vehicles (EVs), You et al. worked diligently to gather datasets from comprehensive dynamic driving profiles over more than a year at different temperatures [109]. A BPNN-based SOH estimate method was then trained using temperature, current, and voltage. In a different study, eight commercial 15-Ah lithium batteries provided the data needed for training and verifying a back-propagation NN SOH model [110]. The impact of completely charged or discharged temperatures (e.g., 25 °C, 45 °C) on calendar life was thoroughly examined. Reference performance tests (RPTs) were conducted for ten months to monitor the degradation trend. The findings show that by calibrating the available capacity at specific conditions, suggested approaches may not only forecast the battery SOH well but also increase accuracy in prediction.

It is commonly known that the caliber of the input features has a significant impact on the model's performance. Therefore, to reduce computational complexity, key traits were chosen in one study using principal component analysis (PCA) [111]. The gathered features were then further broken down and denoised using the complete ensemble empirical mode decomposition with adaptive noise (CEEMDAN) method. A different study created an adaptive adjustable hybrid RBF network that shares most of the characteristics of the autoregressive model [112]. Brownian motion (BM) and PF update the structural parameters, which is the primary benefit of the suggested RBF network. Furthermore, as

an input feature, the Kullback–Leibler distance was calculated using a continuous hidden Markov model (CHMM) and a kernel density estimation (KDE) technique. In the National Aeronautics and Space Administration (NASA) dataset and Center for Advanced Life Cycle Engineering (CALCE) dataset, the suggested adjustable RBF network might achieve better estimation accuracy than the fixed RBF network [113]. Moreover, the suggested approach could retain reliable estimation results even when Gaussian white noise is added to dynamic discharge patterns.

3.1.2. Deep Learning Algorithm

As deep neural networks (DNNs) encompass numerous hidden layers, they excel in efficiently mapping complex and nonlinear functions compared to shallow neural networks. In a specific study, using the smoothing filter, five distinctive characteristics were initially derived from incomplete IC curves [114]. It can be inferred from the Spearman correlation analysis that some of the characteristics were not used as the input vector. The NN model's input was limited to the two feature values with the strongest association with SOH. In addition, the examination of training accuracy and speed indicates that the DNN's final structure is four-layered and has 2–5–6–1 neurons. Five features, including the temperature decrease rate during the CV charging mode, voltage decrease rate during the constant current discharging mode, and voltage increase rate during CC charging mode, form the entire self-made aging dataset to fully cover the battery usage [115]. Every one of the five features exhibited a substantial link with SOH levels, according to the gray relational analysis results. The findings on a 128-neutron layer used in training the estimator show that the maximum estimation accuracy might be achieved by utilizing all five features. In Shi et al.'s (2021) estimate system, the combined use of the model-based EKF approach and the ML DNN method is reviewed in detail [116]. The best model was determined by comparing more than 20 distinct DNN topologies.

Remember that employing a DNN has the advantage of greater accuracy, but it also has the disadvantage of requiring more computer power and longer calculation times.

3.1.3. Support Vector Machine

Because SVM offers a good balance between usability and performance, it is one of the most popular machine learning techniques. Both the conventional SVM model and various SVM versions have been utilized in SOH estimation. It is commonly known that the SVM kernel function can translate the input characteristics implicitly to a high-dimensional feature space in which samples may be separated linearly [117].

The SVM model's hyperparameters were optimized using the differential evolution (DE) technique. The suggested method performed better in terms of both the constant current discharging process and dynamic working circumstances when compared to other machine learning estimating techniques utilizing the NASA dataset. Following an investigation of the impact of the Gaussian kernel's standard deviation (σ) on estimate accuracy, a theory for choosing the appropriate σ was put forward [118].

Another popular technique for optimizing the SVM model is to use more relevant input characteristics. The IC peak values and position [119], constant current charging time, sample entropy [120], energy signal, response of the voltage under pulse test of the current [121], mean and standard deviation of the measured current and voltage, and parameters of ECM [122] are among the frequently used features. To achieve simultaneous optimization of feature extraction and hyperparameter tweaking, a hybrid encoding approach on a single chromosome was employed [121]. A separate study talks about the sliding-window-based feature extraction (SWBFE) [123].

The least-squares support vector machine (LS-SVM) is a significant variation of the regular SVM model with an easier solving procedure. A weighted least-squares technique for estimating SOH was presented in one study and was based on linear equations for retired LiBs and a weighting function [124]. Even in test datasets with varying battery materials and circumstances, the weighted LS-SVM, when compared to the conventional SVM, might enhance the SOH estimate performance by weighting the error factors. Additionally, the PSO method was applied in a different study to enhance optimization [122]. The PSO–LS-SVR approach performed better than the LS-SVR technique without PSO optimization, with an RMSE of less than 2%.

4. Challenges and Prospects

SOC and SOH estimations for electric vehicles (EVs) present a spectrum of intricate challenges and considerations:

4.1. State of Charge Balancing Issues

To meet high voltage and energy needs, hundreds of cells are connected in series or parallel to form the lithium-ion battery (LIB) pack found in electric vehicles (EVs). Because each cell's state of charge (SOC) varies due to physical changes from repeated cycles of charging and discharging, monitoring and measuring SOC across these packs is extremely difficult. SOC variations are caused by constraints in manufacturing methods, material faults, and different operating conditions, which all affect cell performance in terms of capacity and aging. The LIB's overall safety systems may be impacted by these imbalances, as they can significantly impair the quality of data pertaining to power and energy calculations [125]. Recent years have seen the development of a number of ways to solve these problems, such as calculation-based approaches, screening methods, and bias correction tools.

4.2. Charging Strategy

Recent years have seen a significant increase in interest in the charging procedures for LIBs in EVs. Since EVs do not yet have sophisticated fast-charging technologies, the delayed charging procedure could be a deterrent to wider adoption. On the other hand, quick charging techniques that raise the charging current might cause a lot of heat to be produced, which will shorten the battery's lifespan. It is difficult to create a charging method that strikes a compromise between battery durability, thermal control, and charging efficiency. Ref. [126] discuss recent developments in quick charging methods, and Ref. [127] delve deeper on a number of ideal charging approaches.

4.3. Lithium-Ion Battery Material Issue

Despite their generally good performance, lithium-ion batteries' state of charge (SOC) estimation is greatly impacted by the materials employed for the positive and negative electrodes. Despite their good performance, lithium cobalt oxide (LiCo) batteries are expensive and have a limited capacity because of the limited supply of cobalt. Because nickel and cobalt are scarce, lithium nickel manganese cobalt oxide (LiNMC) and lithium nickel cobalt aluminum oxide (LiNCA) batteries, which are renowned for their exceptional performance and longevity, are also expensive. On the other hand, the short lifespan and limited capacity of lithium manganese oxide (LiMO) batteries, which provide high voltage and reasonable safety at a lower cost, are caused by an inadequate supply of manganese. Although lithium iron phosphate (LiFP) batteries are inexpensive, non-toxic, long-lasting, and extremely safe, their low energy production and capacity are their main drawbacks. Though they suffer from capacity and voltage constraints, lithium titanate (LiTO) batteries outperform other lithium-ion kinds in terms of life cycle efficiency and performance. LiTO

can achieve excellent performance and is economically viable in spite of these limitations. As mentioned in reference [128], graphite, which is frequently utilized in negative electrodes, has a poor energy density and inefficiency due to solid electrolyte interface (SEI) development, despite its wide availability and durability.

The SOC was evaluated using two distinct lithium-ion battery chemistries—lithium titanate (LTO) and lithium iron phosphate (LiFePO4)—under various aging profiles and temperatures in a comparative study referenced in [129]. According to the results, LiFePO4 batteries have an RMSE of 0.50305% at 25 °C, whereas LTO batteries exhibit an RMSE of 0.7012%. Additionally, the study showed that LiFePO4 batteries deteriorate considerably with prolonged cycling, with an RMSE rising to 0.4547% after 1000 cycles, while LTO batteries exhibit greater aging resistance, maintaining a constant RMSE of 0.00334% after the same number of cycles.

4.4. Hardware Development for Real-Time SOC Monitoring

Thus far, experimental testing across a range of temperature conditions, noise effects, and beginning SOC levels has been used to validate SOC estimate techniques. Despite these initiatives, there is still a dearth of thorough research on SOC estimation for LIBs operating in real-world scenarios. Implementing SOC estimation techniques in a BMS that must strike a balance between low cost, limited memory capacity, and fast computational speed is a significant problem. In order to test an adaptive Hoo-filter-based SOC estimate algorithm in real-time settings, a hardware-in-the-loop (HIL) experimental platform was created [130]. Similarly, a lithium-ion battery-in-loop testing apparatus was built and benched with an xPC target to verify a multiscale dual Hoo filter for real-time SOC and capacity estimation and to mimic electric vehicle (EV) drive cycles [131]. In one study's evaluation of SOC using a system-in-the-loop configuration for lithium batteries, a field-programmable gate array (FPGA)-based BMS attained a remarkably quick execution time of 16.5 microseconds and compatibility with inexpensive hardware [132]. Furthermore, battery state estimators were evaluated on an FPGA-based BMS using an HIL platform. Beyond the technological difficulties noted above, a number of factors, including battery aging, model variations, hysteresis, cell unbalancing, self-discharge, and the rate of charge–discharge currents, affect the accuracy of SOC estimates. Prior studies have examined these issues in great depth [128].

4.5. Data Quality

Large amounts of data are essential for ML state estimate techniques. For them to succeed, obtaining high-quality datasets is also essential.

First, the accuracy of the data determines how reliable high-quality datasets are. Usually, advanced battery testing devices with a controller, programmable load, and an integrated software system within the host computer are used to gather these statistics. The Arbin BT2000 [133] and the NEWARE BTS series are examples of common battery testing platforms. Data quality and the efficacy of machine learning algorithms are significantly impacted by variations in these testing platforms, including variations in data collecting speed and accuracy. Therefore, advanced battery testing systems are essential for lowering measurement noise and offering a solid foundation for model training and validation. Furthermore, the volume of data gathered also affects the datasets' quality. Theoretically, expanding the training data can improve the generalization of DL algorithms and reduce problems like model overfitting. Since LiBs are affected by their operating environment, the quality of training data has a major impact on how well ML algorithms work in EVs and associated subsystems.

Thirdly, high-quality databases require a diversity of data. Although controlled laboratory simulations can produce a large amount of data, they do not offer much variety. Data from laboratory settings using common tests, such as constant charge or discharge and dynamic drive cycles, have been used in the majority of research. Only a small number of studies, though, have included data from real EV usage [134]. These real-world datasets are essential for training machine learning models, because they introduce changes in patterns that are different from lab simulations. Additional data types greatly increase the diversity of the datasets. These include temperature changes detected by resistance temperature detectors (RTD) [135], volumetric changes measured by optical fiber bragging (FBG) sensors [136], and internal temperatures measured by thermocouples.

In conclusion, improving training data's accuracy, quantity, and variety is a basic but crucial task for the advancement of machine learning algorithms in the future.

4.6. Hyperparameter Tuning and Structure Selection

Because network design and hyperparameter selection have an impact on the ML algorithm's performance, choosing the best structure and fine-tuning hyperparameters are additional difficult challenges. Consider the neural network (NN) as an example. Generally speaking, the more complicated the structure, the more parameters that must be taught. The computing load needed to train and run the model increases with the number of hidden layers. Up until now, the majority of architecture choices has been limited to the time-consuming and ineffective trial-and-error method. For instance, a singular value decomposition technique could be used to determine the number of hidden-layer neurons [137]. There is currently no standardized approach that can be used to direct the selection of appropriate hyperparameters for variously specific problems, hyperparameters which include the learning rate, neuron initialization, optimization algorithm, dropouts, batch size, batch normalization, and activation function. As a result, the trial-and-error method is also used to adjust the hyperparameters until acceptable outcomes are obtained. Several studies showed that the algorithm's performance will be greatly impacted by various hyperparameter settings [68,138]. They also compared the algorithm's performance under various hyperparameter settings.

There must be greater focus on how ML algorithms have been compared, because choosing an architecture and fine-tuning hyperparameters are the most time-consuming tasks for ML algorithms. With many approaches to improve SBS (sequential backward selection), many attempts at hyperparameter tuning are skewed by the small number of heuristic optimization techniques that are known to be effective. While optimization techniques like SA (simulated annealing) and SGD (stochastic gradient descent) are mainly theoretical, widely utilized heuristics like genetic algorithms (GAs) are thought to be unreliable methods of testing heuristic optimization strategies.

These methods can also be slow, and there are still few clear applications for them. The main drawbacks of machine learning algorithms that employ these optimization strategies are their slow convergence, which can be critical, and their laborious parameter adjustment, which can impair the algorithms' performance. Furthermore, there has not been sufficient comparison between the heuristic optimization methods used in hyperparameter tuning mentioned above. As a result, future research must enhance the ML algorithm's hyperparameter tweaking and optimal structure selection.

4.7. Hybrid Algorithms and Ensemble Learning

For the estimation of SOC or SOH, recent studies have mostly used a single approach. Nonetheless, hybrid algorithms—which blend several algorithms—have become more and more well-liked for improving accuracy, resilience, and efficiency. These hybrid algo-

rithms, which are typically divided into two categories—those that combine model-based techniques with ML methods and those that integrate several ML methods—use the advantages of multiple approaches to provide better results. To improve the accuracy and resilience of SOC estimate techniques, for example, more sophisticated filters like EKF, UKF, and adaptive UKF are frequently combined with simpler neural network forms like BPNN, RBFNN, and ELM. Optimization via UKF and particle filter (PF) is advantageous for deep learning algorithms such as DNN, NARXNN, and LSTM. Additionally, the combination of other machine learning models, such as CNN with GRU or LSTM, leverages the strength of RNN's sequence prediction and CNN's feature extraction capabilities. Additionally, methods such as Gaussian process regression (GPR) and RBFNN [111] have been used with linear regression to improve SOC estimation accuracy. Another useful method to raise training precision, effectiveness, and model resilience is ensemble learning (EL). By cleverly mixing multiple distinct algorithms, EL aims to reduce the risks associated with single algorithms that perform badly [139]. Random forest (RF) is a popular ensemble approach that uses decision-tree logic and a bagging technique. Approximately two-thirds of the original dataset size is used in bootstrapping to create training datasets, with the remaining unselected samples included as out-of-bag (OOB) samples. These datasets are then utilized to generate several decision trees, and performance is assessed using the OOB samples. A random forest (RF) is produced by combining the results of several decision trees. In order to estimate battery capacity, for instance, Li et al. created an RF model with multiple trees [140]. They did this by immediately entering raw data, such as current, voltage, and time, into the model without any preprocessing. This resulted in a minimal computing demand and resulting estimates with an RMSE of less than 1.3%. Another study evaluated the classifier against decision trees and RF using time-related variables collected from charge–discharge cycles [141]. The results showed that RF performed better than other models in general because of its thorough approach to battery capacity estimation.

4.8. Evaluation and Implementation of the Algorithm

In future research, thorough assessment and on-device implementation of ML techniques will be essential. First, consistent training, validation, and testing datasets are essential for evaluating an ML method, especially when compared to other algorithms. SOC and SOH estimation models are built using publicly accessible datasets [142–144]. Furthermore, since computational needs and memory storage are directly related to model complexity, it is preferable to align the complexity of models (e.g., count of trainable parameters, selected training techniques) across the algorithms under comparison. Other factors that need to be taken into account in addition to model accuracy include model robustness against various uncertainties, training duration, memory usage, floating point operations per second (FLOPs), and parameter count [145,146]. In the development of machine learning algorithms, finding the ideal balance between model complexity and accuracy continues to be a major problem. Future studies should therefore evaluate ML approaches using a multifaceted analytical framework.

Second, prior research has usually used the same kind of battery for both model evaluation and training. However, the performance of the pretrained ML models frequently deteriorates when these models are applied to batteries with differences in their parameters, such as their capacity or electrode material. Furthermore, collecting fresh training data and retraining models for each type of battery is not feasible. There is a need for more research to improve the adaptability of ML approaches across many battery situations, as recent studies have investigated the application of transfer learning techniques to adapt ML methods to different battery types [147,148].

Finally, the significant computational overhead of ML methods for state estimation has hindered their in situ implementation. However, embedding ML algorithms directly onto devices is a feasible option for next-generation battery management systems (BMS) due to developments in big data analytics, 5G network capabilities, cloud computing infrastructures, and other new technologies. Cloud computing provides the scalability to handle huge data quantities, while the emergence of big data and the Internet of Things (IoT) offers the enormous datasets required for machine learning applications. Additionally, the computational effort related to offline machine learning training is decreased by the wider availability of graphic processing units (GPUs). From a different angle, ongoing online training of machine learning algorithms is crucial, particularly for batteries.

The effectiveness of statically trained state estimation models decreases with the age of LiBs. As a result, ML algorithms that are directly installed on devices are able to learn and adjust in real time under real-world operating conditions. This allows for continuous enhancements and prompt implementation of insights obtained from EV usage data.

4.9. Thermal Influences

Given the acute sensitivity of battery performance to thermal conditions, SOC and SOH evaluations are particularly susceptible to deviations in ambient and operational temperatures, necessitating the incorporation of advanced modeling techniques to mitigate these effects.

4.10. Sensor Constraints and Economic Factors

The reliance on high-precision sensors for accurate measurements introduces constraints, not only in terms of the financial outlay but also in the limitations inherent in sensor technologies.

In summation, the process of estimating the state of charge and health in EVs encompasses a range of technical, computational, and practical challenges, necessitating ongoing innovations in battery technology, data analytics, and algorithmic development to enhance the efficacy and reliability of these estimations.

5. Conclusions

SOC and SOH estimate techniques are evaluated critically in this review and divided into model-based and data-driven methodologies. While data-driven approaches are superior when system details are unclear, model-based approaches perform better statistically when system models are predefined. These tactics are currently being integrated in research to maximize their advantages, especially in light of data availability and computational developments.

The review identifies many shortcomings in the methods used for SOC and SOH estimation today:

- Aging, discharge rates, and sensor precision all have an impact on the accumulated mistakes that plague coulomb counting.
- The OCV method's flat SOC–OCV curve segment makes it inaccurate for LiFePO4 batteries and inapplicable in real time for EVs.
- The computing requirement and parameter estimation time provide difficulties for EM and ECM.
- Complex operations and sensitivity to model errors are KF's limitations.
- NN requires extensive training, yet it produces reliable estimates in a variety of scenarios.
- The computational complexity and optimization difficulties of FL, ANFIS, GA, and PSO place limitations on them.

ML techniques approaches to SOC and SOH estimation are also well covered in this review. There has been insufficient in-depth study of ML techniques; by offering a thorough and organized analysis of the machine learning techniques used for SOC and SOH estimates, this work seeks to close this research gap. This review's initial contribution outlines the standard procedures for SOC and SOH estimation, describing the basic ideas of popular machine learning algorithm types—deep learning (DL), support vector machines (SVM), shallow neural networks (NN), and Gaussian process regression (GPR)—along with their mathematical formulas and visual representations to aid their comprehension.

Specific methods such as CNN, LSTM, extreme learning machines (ELM), and BPNN are covered in detail. Another significant contribution is the review's methodical analysis of common uses of these machine learning categories in SOC and SOH estimation, which includes a thorough summary of specifics like input features, datasets utilized, hyperparameter selection, and performance metrics in extensive tables for easy reference and comparison. Furthermore, a critical analysis is conducted of the benefits, limitations, and similarities among various uses of these algorithms.

Highlighting issues including data quality, structure selection, hyperparameter tuning, hybrid frameworks, and algorithm execution, this review examines the main obstacles and potential future developments of ML-based state estimation techniques. Significant avenues for future research are suggested, with an emphasis on improving the precision, abundance, and diversity of data; optimizing structure selection and hyperparameter adjustments; utilizing advanced learning strategies to increase the accuracy and robustness of models; assessing machine learning techniques in various dimensions; and integrating ML state estimation techniques onboard.

Adding to previous observations, this analysis also points out that although ML algorithms for SOC and SOH estimation show a great deal of promise for future advancements in BMS, they also confront several real-world difficulties. Future studies should focus on technologies that use cloud computing and online retraining, create fusion models and joint multistate estimates, anticipate whole life cycles, improve data variety through advanced sensing, and make onboard installation easier. By addressing both present constraints and potential future developments, this thorough study seeks to motivate academics to further the use of ML algorithms in SOC and SOH estimates.

The following are suggestions for additional research:

- Thorough research on electrochemical models to comprehend the dynamics and degradation of batteries.
- Creation of efficient SOC and SOH management controllers and real-time SOC and SOH estimation systems.
- Optimization-based reduction of computing complexity in data-driven approaches.

In summary, while significant strides have been made in battery technology and management for EVs, accurately estimating SOC and SOH remains a complex challenge. Addressing this requires a multifaceted approach, including ongoing research, advanced algorithm development, leveraging machine learning, and continuous calibration and validation efforts.

Author Contributions: Conceptualization, B.D.S. and I.B.; methodology, B.D.S., M.V.A.D. and T.B.; software, B.D.S. and M.V.A.D.; validation, I.B., M.V.A.D. and T.B.; formal analysis, B.D.S. and T.B.; investigation, B.D.S., M.V.A.D. and T.B.; resources, I.B.; data curation, B.D.S. and M.V.A.D.; writing—original draft preparation, B.D.S.; writing—review and editing, B.D.S., I.B., M.V.A.D. and T.B.; visualization, B.D.S. and T.B.; supervision, I.B.; funding acquisition, I.B. All authors have read and agreed to the published version of the manuscript.

Funding: This research received no external funding.

Data Availability Statement: No new data were created or analyzed in this study. Data sharing is not applicable to this article, as this is a review of existing literature.

Acknowledgments: B.D.S would like to express his gratitude to Tennessee Technological University for providing the resources and support required for this research. Special thanks to Indranil Bhattacharya for his invaluable guidance and mentorship throughout the development of this paper. B.D.S. also acknowledges the contributions of Mary Vinolisha Anthony Dhason and Trapa Banik for their insightful discussions and feedback.

Conflicts of Interest: The authors declare no conflicts of interest.

References

1. Ramoni, M.O.; Zhang, H.-C. End-of-life (EOL) issues and options for electric vehicle batteries. *Clean Technol. Environ. Policy* **2013**, *15*, 881–891. [CrossRef]
2. Hu, X.; Zou, C.; Zhang, C.; Li, Y. Technological developments in batteries: A survey of principal roles, types, and management needs. *IEEE Power Energy Mag.* **2017**, *15*, 20–31. [CrossRef]
3. Xiong, R.; He, H.; Sun, F.; Zhao, K. Online estimation of peak power capability of Li-Ion batteries in electric vehicles by a hardware-in-loop approach. *Energies* **2012**, *5*, 1455–1469. [CrossRef]
4. Xing, Y.; Ma, E.W.M.; Tsui, K.L.; Pecht, M. Battery management systems in electric and hybrid vehicles. *Energies* **2011**, *4*, 1840–1857. [CrossRef]
5. Lillehei, C.; Cruz, A.B.; Johnsrude, I.; Sellers, R.D. A new method of assessing the state of charge of implanted cardiac pacemaker batteries. *Am. J. Cardiol.* **1965**, *16*, 717–721. [CrossRef]
6. Hannan, M.A.; Lipu, M.S.H.; Hussain, A.; Mohamed, A. A review of lithium-ion battery state of charge estimation and management system in electric vehicle applications: Challenges and recommendations. *Renew. Sustain. Energy Rev.* **2017**, *78*, 834–854. [CrossRef]
7. Li, Z.; Huang, J.; Liaw, B.Y.; Zhang, J. On state-of-charge determination for lithium-ion batteries. *J. Power Sources* **2017**, *348*, 281–301. [CrossRef]
8. Kalawoun, J.; Biletska, K.; Suard, F.; Montaru, M. From a novel classification of the battery state of charge estimators toward a conception of an ideal one. *J. Power Sources* **2015**, *279*, 694–706. [CrossRef]
9. Lu, L.; Han, X.; Li, J.; Hua, J.; Ouyang, M. A review on the key issues for lithium-ion battery management in electric vehicles. *J. Power Sources* **2013**, *226*, 272–288. [CrossRef]
10. Plett, G.L. *Battery Management and Control*; ECE5720, Lecture Notes, Note 3; Artech House: Norwood, MA, USA, 2015; p. 7.
11. Baccouche, I.; Jemmali, S.; Manai, B.; Omar, N.; Ben Amara, N.E. Improved OCV model of a Li-ion nmc battery for online SOC estimation using the extended Kalman filter. *Energies* **2017**, *10*, 764. [CrossRef]
12. Lin, C.; Yu, Q.; Xiong, R.; Wang, L.Y. A study on the impact of open circuit voltage tests on state of charge estimation for lithium-ion batteries. *Appl. Energy* **2017**, *205*, 892–902. [CrossRef]
13. Liu, K.; Li, K.; Peng, Q.; Zhang, C. A brief review on key technologies in the battery management system of electric vehicles. *Front. Mech. Eng.* **2018**, *14*, 47–64. [CrossRef]
14. Zhang, B.; Lu, C.; Liu, J. Combination Algorithm for State of Charge Estimation. In Proceedings of the 2013 International Conference on Communication Systems and Network Technologies (CSNT 2013), Gwalior, India, 6–8 April 2013; pp. 865–867.
15. Wenzel, M.J.; Drees, K.H.; Elbsat, M.N. Electrical Energy Storage System with Variable State-of-Charge Frequency Response Optimization. U.S. Patent 10186889B2, 22 January 2019.
16. Grandjean, T.R.B.; McGordon, A.; Jennings, P.A. Structural identifiability of equivalent circuit models for Li-ion batteries. *Energies* **2017**, *10*, 90. [CrossRef]
17. Tang, S.-X.; Camacho-Solorio, L.; Wang, Y.; Krstic, M. State-of-charge estimation from a thermal–electrochemical model of lithium-ion batteries. *Automatica* **2017**, *83*, 206–219. [CrossRef]
18. Li, J.; Wang, L.; Lyu, C.; Pecht, M. State of charge estimation based on a simplified electrochemical model for a single $LiCoO_2$ battery and battery pack. *Energy* **2017**, *133*, 572–583. [CrossRef]
19. Wang, Y.; Zhang, C.; Chen, Z. On-line battery state-of-charge estimation based on an integrated estimator. *Appl. Energy* **2017**, *185*, 2026–2032. [CrossRef]
20. Zou, C.; Manzie, C.; Nešić, D.; Kallapur, A.G. Multi-time-scale observer design for state-of-charge and state-of-health of a lithium-ion battery. *J. Power Sources* **2016**, *335*, 121–130. [CrossRef]
21. Xiong, B.; Zhao, J.; Su, Y.; Wei, Z.; Skyllas-Kazacos, M. State of charge estimation of vanadium redox flow battery based on sliding mode observer and dynamic model including capacity fading factor. *IEEE Trans. Sustain. Energy* **2017**, *8*, 1658–1667. [CrossRef]
22. Ye, M.; Guo, H.; Cao, B. A model-based adaptive state of charge estimator for a lithium-ion battery using an improved adaptive particle filter. *Appl. Energy* **2017**, *190*, 740–748. [CrossRef]

23. Plett, G.L. *Battery Management and Control*; ECE5720, Lecture Notes, Note 2; Artech House: Norwood, MA, USA, 2015; p. 10.
24. Kalman, R.E. A new approach to linear filtering and prediction problems. *J. Basic Eng.* **1960**, *82*, 35–45. [CrossRef]
25. Plett, G.L. Kalman-Filter SOC Estimation for LiPB HEV Cells. In Proceedings of the 19th International Battery, Hybrid and Fuel Cell Electric Vehicle Symposium & Exhibition (EVS19), Busan, Republic of Korea, 19–23 October 2002; p. 3.
26. Plett, G.L. Kalman-Filter SOC Estimation for LiPB HEV Cells. In Proceedings of the 19th International Battery, Hybrid and Fuel Cell Electric Vehicle Symposium & Exhibition (EVS19), Busan, Republic of Korea, 19–23 October 2002; p. 4.
27. Haykin, S. (Editor) Kalman Filtering and Neural Networks; Wiley Inter-Science: New York, NY, USA, 2001.
28. Plett, G.L. Kalman-Filter SOC Estimation for LiPB HEV Cells. In Proceedings of the 19th International Battery, Hybrid and Fuel Cell Electric Vehicle Symposium & Exhibition (EVS19), Busan, Republic of Korea, 19–23 October 2002; p. 5.
29. Rahman, A.; Anwar, S.; Izadian, A. Electrochemical model parameter identification of a lithium-ion battery using particle swarm optimization method. *J. Power Sources* **2016**, *307*, 86–97. [CrossRef]
30. Sung, W.; Shin, C.B. Electrochemical model of a lithium-ion battery implemented into an automotive battery management system. *Comput. Chem. Eng.* **2015**, *76*, 87–97. [CrossRef]
31. Peng, S.; Chen, C.; Shi, H.; Yao, Z. State of charge estimation of battery energy storage systems based on adaptive unscented Kalman filter with a noise statistics estimator. *IEEE Access* **2017**, *5*, 13202–13212. [CrossRef]
32. Mastali, M.; Samadani, E.; Farhad, S.; Fraser, R.; Fowler, M. Three-dimensional multiparticle electrochemical model of $LiFePO_4$ cells based on a resistor network methodology. *Electrochim. Acta* **2016**, *190*, 574–587. [CrossRef]
33. Zou, C.; Manzie, C.; Nesic, D. A framework for simplification of PDE-based lithium-ion battery models. *IEEE Trans. Control. Syst. Technol.* **2015**, *24*, 1594–1609. [CrossRef]
34. Bartlett, A.; Marcicki, J.; Onori, S.; Rizzoni, G.; Yang, X.G.; Miller, T. Electrochemical model-based state of charge and capacity estimation for a composite electrode lithium-Ion battery. *IEEE Trans. Control Syst. Technol.* **2015**, *24*, 384–399. [CrossRef]
35. Zhang, L.; Wang, Z.; Hu, X.; Sun, F.; Dorrell, D.G. A comparative study of equivalent circuit models of ultracapacitors for electric vehicles. *J. Power Sources* **2015**, *274*, 899–906. [CrossRef]
36. Zhang, X.; Lu, J.; Yuan, S.; Yang, J.; Zhou, X. A novel method for identification of lithium-ion battery equivalent circuit model parameters considering electrochemical properties. *J. Power Sources* **2017**, *345*, 21–29. [CrossRef]
37. Widanage, W.D.; Barai, A.; Chouchelamane, G.H.; Uddin, K.; McGordon, A.; Marco, J.; Jennings, P. Design and use of multisite signals for Li-ion battery equivalent circuit modeling. Part 1: Signal design. *J. Power Sources* **2016**, *324*, 70–78. [CrossRef]
38. Wang, Q.-K.; He, Y.-J.; Shen, J.-N.; Ma, Z.-F.; Zhong, G.-B. A unified modeling framework for lithium-ion batteries: An artificial neural network based thermal coupled equivalent circuit model approach. *Energy* **2017**, *138*, 118–132. [CrossRef]
39. Deng, Z.; Yang, L.; Cai, Y.; Deng, H.; Sun, L. Online available capacity prediction and state of charge estimation based on advanced da-ta-driven algorithms for lithium iron phosphate battery. *Energy* **2016**, *112*, 469–480. [CrossRef]
40. Plett, G.L. *Battery Management and Control*; ECE5720, Lecture Notes, Note 2; Artech House: Norwood, MA, USA, 2015; pp. 8–9.
41. Lee, S.; Kim, J.; Lee, J.; Cho, B. State-of-charge and capacity estimation of lithium-ion battery using a new open-circuit voltage versus state-of-charge. *J. Power Sources* **2008**, *185*, 1367–1373. [CrossRef]
42. Idaho National Engineering; Environmental Laboratory. *Battery Test Manual for Plug-In Hybrid Electric Vehicles*; Assistant Secretary for Energy Efficiency and Renewable Energy (EE); Idaho Operations Office: Idaho Falls, ID, USA, 2010.
43. Lee, E.R.; Noh, H.; Park, B.U. Model selection via Bayesian information criterion for quantile regression models. *J. Am. Stat. Assoc.* **2014**, *109*, 216–229. [CrossRef]
44. Hu, M.; Li, Y.; Li, S.; Fu, C.; Qin, D.; Li, Z. Lithium-ion battery modeling and parameter identification based on fractional theory. *Energy* **2018**, *165*, 153–163. [CrossRef]
45. Zhang, J.; Wang, P.; Liu, Y.; Cheng, Z. Variable-Order Equivalent Circuit Modeling and State of Charge Estimation of Lithium-Ion Battery Based on Electrochemical Impedance Spectroscopy. *Energies* **2021**, *14*, 769. [CrossRef]
46. Xu, J.; Mi, C.C.; Cao, B.; Cao, J. A new method to estimate the state of charge of lithium-ion batteries based on the battery impedance model. *J. Power Sources* **2013**, *233*, 277–284. [CrossRef]
47. Li, M. Li-ion dynamics and state of charge estimation. *Renew. Energy* **2017**, *100*, 44–52. [CrossRef]
48. Di Domenico, D.; Stefanopoulou, A.; Fiengo, G. Lithium-ion battery state of charge and critical surface charge estimation using an electrochemical model-based extended Kalman filter. *J. Dyn. Syst. Meas. Control* **2010**, *132*, 061302. [CrossRef]
49. Cacciato, M.; Nobile, G.; Scarcella, G.; Scelba, G. Real-time model-based estimation of SoC and SOH for energy storage systems. *IEEE Trans. Power Electron.* **2017**, *32*, 794–803. [CrossRef]
50. Ye, M.; Guo, H.; Xiong, R.; Yang, R. Model-based state-of-charge estimation approach of the lithium-ion battery using an improved adaptive particle filter. *Energy Procedia* **2016**, *103*, 394–399. [CrossRef]
51. Xiong, R.; Cao, J.; Yu, Q.; He, H.; Sun, F. Critical review on the battery state of charge estimation methods for electric vehicles. *IEEE Access* **2017**, *6*, 1832–1843. [CrossRef]
52. Dai, H.; Jiang, B.; Wei, X. Impedance characterization and modeling of lithium-ion batteries considering the internal temperature gradient. *Energies* **2018**, *11*, 220. [CrossRef]

53. Chemali, E.; Kollmeyer, P.J.; Preindl, M.; Emadi, A. State-of-charge estimation of Li-ion batteries using deep neural networks: A machine learning approach. *J. Power Sources* **2018**, *400*, 242–255. [CrossRef]
54. Lipu, M.S.H.; Hannan, M.A.; Hussain, A.; Saad, M.H.; Ayob, A.; Uddin, M.N. Extreme learning machine model for state-of-charge estimation of lithium-ion battery using gravitational search algorithm. *IEEE Trans. Ind. Appl.* **2019**, *55*, 4225–4234. [CrossRef]
55. Hu, X.; Li, S.E.; Yang, Y. Advanced machine learning approach for lithium-ion battery state estimation in ELECTRIC VEHICLES. *IEEE Trans. Transp. Electrif.* **2015**, *2*, 140–149. [CrossRef]
56. Giger, M.L. Machine learning in medical imaging. *J. Amer. Coll. Radiol.* **2018**, *15*, 512–520. [CrossRef]
57. Chatzis, S.P.; Siakoulis, V.; Petropoulos, A.; Stavroulakis, E.; Vlachogiannakis, N. Forecasting stock market crisis events using deep and statistical machine learning techniques. *Expert Syst. Appl.* **2018**, *112*, 353–371. [CrossRef]
58. Xu, Y.; Yang, C.; Zhong, J.; Wang, N.; Zhao, L. Robot teaching by teleoperation based on visual interaction and extreme learning machine. *Neurocomputing* **2017**, *275*, 2093–2103. [CrossRef]
59. Silver, D.; Huang, A.; Maddison, C.J.; Guez, A.; Sifre, L.; van den Driessche, G.; Schrittwieser, J.; Antonoglou, I.; Panneershelvam, V.; Lanctot, M.; et al. Mastering the game of Go with deep neural networks and tree search. *Nature* **2016**, *529*, 484–489. [CrossRef]
60. Anand, I.; Mathur, B. State of charge estimation of lead acid batteries using neural networks. In Proceedings of the 2013 International Conference on Circuits, Power and Computing Technologies (ICCPCT), Nagercoil, India, 20–21 March 2013; pp. 596–599.
61. Chen, J.; Longhui, W.; Wu, C.; Yiheng, Z. Method for Estimating State of Charge of Battery. WO Patent 2019052015A1, 21 March 2019.
62. Hannan, M.A.; Lipu, M.S.H.; Hussain, A.; Saad, M.H.; Ayob, A. Neural network approach for estimating state of charge of lithium-ion battery using backtracking search algorithm. *IEEE Access* **2018**, *6*, 10069–10079. [CrossRef]
63. Hongwei, L.; Caiying, S. Methods of State of Charge Estimation of Electric Vehicle. *Automot. Eng.* **2017**, 31–33.
64. Xia, B.; Cui, D.; Sun, Z.; Lao, Z.; Zhang, R.; Wang, W.; Sun, W.; Lai, Y.; Wang, M. State of charge estimation of lithium-ion batteries using optimized Levenberg-Marquardt wavelet neural network. *Energy* **2018**, *153*, 694–705. [CrossRef]
65. Schmidhuber, J. Deep learning in neural networks: An overview. *Neural Netw.* **2015**, *61*, 85–117. [CrossRef] [PubMed]
66. He, W.; Williard, N.; Chen, C.; Pecht, M. State of charge estimation for Li-ion batteries using neural network modeling and unscented Kalman filter-based error cancellation. *Int. J. Electr. Power Energy Syst.* **2014**, *62*, 783–791. [CrossRef]
67. Crocioni, G.; Pau, D.; Delorme, J.-M.; Gruosso, G. Li-ion batteries parameter estimation with tiny neural networks embedded on intelligent IoT microcontrollers. *IEEE Access* **2020**, *8*, 122135–122146. [CrossRef]
68. Song, X.; Yang, F.; Wang, D.; Tsui, K.-L. Combined CNN-LSTM network for state-of-charge estimation of lithium-ion batteries. *IEEE Access* **2019**, *7*, 88894–88902. [CrossRef]
69. Huang, Z.; Yang, F.; Xu, F.; Song, X.; Tsui, K.-L. Convolutional gated recurrent unit–recurrent neural network for state-of-charge estimation of lithium-ion batteries. *IEEE Access* **2019**, *7*, 93139–93149. [CrossRef]
70. Hannan, M.A.; How, D.N.T.; Lipu, M.S.H.; Ker, P.J.; Dong, Z.Y.; Mansur, M.; Blaabjerg, F. SOC estimation of Li-ion batteries with learning rate-optimized deep fully convolutional network. *IEEE Trans. Power Electron.* **2020**, *36*, 7349–7353. [CrossRef]
71. Hu, J.; Hu, J.; Lin, H.; Li, X.; Jiang, C.; Qiu, X.; Li, W. State-of-charge estimation for battery management system using optimized support vector machine for regression. *J. Power Sources* **2014**, *269*, 682–693. [CrossRef]
72. Jiménez-Bermejo, D.; Fraile-Ardanuy, J.; Castaño-Solis, S.; Merino, J.; Álvaro-Hermana, R. Using dynamic neural networks for battery state of charge estimation in electric vehicles. *Procedia Comput. Sci.* **2018**, *130*, 533–540. [CrossRef]
73. Lipu, M.S.H.; Hussain, A.; Saad, M.H.M.; Ayob, A.; Hannan, M.A. Improved recurrent NARX neural network model for state of charge estimation of lithium-ion battery using pso algorithm. In Proceedings of the 2018 IEEE Symposium on Computer Applications & Industrial Electronics (ISCAIE), Penang, Malaysia, 28–29 April 2018; pp. 354–359.
74. Sun, W.; Qiu, Y.; Sun, L.; Hua, Q. Neural network-based learning and estimation of batterystate-of-charge: A comparison study between direct and indirect methodology. *Int. J. Energy Res.* **2020**, *44*, 10307–10319. [CrossRef]
75. Qin, X.; Gao, M.; He, Z.; Liu, Y. State of charge estimation for lithium-ion batteries based on NARX neural network and UKF. In Proceedings of the 2019 IEEE 17th International Conference on Industrial Informatics (INDIN), Helsinki-Espoo, Finland, 22–25 July 2019; pp. 1706–1711.
76. Wang, Q.; Gu, H.; Ye, M.; Wei, M.; Xu, X. State of charge estimation for lithium-ion battery based on NARX recurrent neural network and moving window method. *IEEE Access* **2021**, *9*, 83364–83375. [CrossRef]
77. Vapnik, V. The Support Vector Method of Function Estimation. In *Nonlinear Modeling*; Springer: Boston, MA, USA, 1998; pp. 55–85. [CrossRef]
78. Fletcher, T. Support vector machines explained. *Tutor. Pap.* **2009**, *1118*, 1–19. Available online: http://sutikno.blog.undip.ac.id/files/2011/11/SVM-Explained.pdf (accessed on 12 January 2025).
79. Antón, J.C.; Nieto, P.J.G.; Viejo, C.B.; Vilán, J.A.V. Support vector machines used to estimate the battery state of charge. *IEEE Trans. Power Electron.* **2013**, *28*, 5919–5926. [CrossRef]

80. Li, R.; Xu, S.; Li, S.; Zhou, Y.; Zhou, K.; Liu, X.; Yao, J. State of charge prediction algorithm of lithium-ion battery based on PSO-SVR cross validation. *IEEE Access* **2020**, *8*, 10234–10242. [CrossRef]
81. Novák, V.; Perfilieva, I.; Močkoř, J. Functional systems in fuzzy logic theories. In *Mathematical Principles of Fuzzy Logic*; Springer: Boston, MA, USA, 1999; pp. 179–222.
82. Salkind, A.J.; Fennie, C.; Singh, P.; Atwater, T.; E Reisner, D. Determination of state-of-charge and state-of-health of batteries by fuzzy logic methodology. *J. Power Sources* **1999**, *80*, 293–300. [CrossRef]
83. Sheng, H.; Xiao, J. Electric vehicle state of charge estimation: Nonlinear correlation and fuzzy support vector machine. *J. Power Sources* **2015**, *281*, 131–137. [CrossRef]
84. Li, Y.; Wang, C.; Gong, J. A combination Kalman filter approach for state of charge estimation of lithium-ion battery considering model uncertainty. *Energy* **2016**, *109*, 933–946. [CrossRef]
85. Singh, P.; Vinjamuri, R.; Wang, X.; Reisner, D. Design and implementation of a fuzzy logic-based state-of-charge meter for Li-ion batteries used in portable defibrillators. *J. Power Sources* **2006**, *162*, 829–836. [CrossRef]
86. Awadallah, M.A.; Venkatesh, B. Accuracy improvement of SoC estimation in lithium-ion batteries. *J. Energy Storage* **2016**, *6*, 95–104. [CrossRef]
87. Zahid, T.; Xu, K.; Li, W.; Li, C.; Li, H. State of charge estimation for electric vehicle power battery using advanced machine learning algorithm under diversified drive cycles. *Energy* **2018**, *162*, 871–882. [CrossRef]
88. Shen, W.; Chan, C.; Lo, E.; Chau, K. Adaptive neurofuzzy modeling of battery residual capacity for electric vehicles. *IEEE Trans. Ind. Electron.* **2002**, *49*, 677–684. [CrossRef]
89. Arabmakki, E.; Kantardzic, M. SOM-based partial labeling of imbalanced data stream. *Neurocomputing* **2017**, *262*, 120–133. [CrossRef]
90. Coleman, M.; Hurley, W.G.; Lee, C.K. An improved battery characterization method using a two-pulse load test. *IEEE Trans. Energy Convers.* **2008**, *23*, 708–713. [CrossRef]
91. Roscher, M.A.; Assfalg, J.; Bohlen, O.S. Detection of utilizable capacity deterioration in battery systems. *IEEE Trans. Veh. Technol.* **2010**, *60*, 98–103. [CrossRef]
92. Zhang, J.; Lee, J. A review on prognostics and health monitoring of Li-ion battery. *J. Power Sources* **2011**, *196*, 6007–6014. [CrossRef]
93. Xiong, R.; Tian, J.; Mu, H.; Wang, C. A systematic model-based degradation behavior recognition and health monitoring method for lithium-ion batteries. *Appl. Energy* **2017**, *207*, 372–383. [CrossRef]
94. Berecibar, M.; Gandiaga, I.; Villarreal, I.; Omar, N.; Van Mierlo, J.; van den Bossche, P. Critical review of state of health estimation methods of Li-ion batteries for real applications. *Renew. Sustain. Energy Rev.* **2016**, *56*, 572–587. [CrossRef]
95. Nejad, S.; Gladwin, D.; Stone, D. A systematic review of lumped-parameter equivalent circuit models for real-time estimation of lithium-ion battery states. *J. Power Sources* **2016**, *316*, 183–196. [CrossRef]
96. Wang, D.; Yang, F.; Tsui, K.-L.; Zhou, Q.; Bae, S.J. Remaining useful life prediction of lithium-ion batteries based on spherical cubature particle filter. *IEEE Trans. Instrum. Meas.* **2016**, *65*, 1282–1291. [CrossRef]
97. Plett, G.L. Sigma-point Kalman filtering for battery management systems of LiPB-based HEV battery packs: Part 1: Intro-duction and state estimation. *J. Power Sources* **2006**, *161*, 1356–1368. [CrossRef]
98. Hu, C.; Youn, B.D.; Chung, J.S.; Ortanez, R. A multiscale framework with extended kalman filter for lithium-ion battery SOC and capacity estimation. *ECS Meet. Abstr.* **2010**, *92*, 694–704. [CrossRef]
99. Wang, J.; Liu, P.; Hicks-Garner, J.; Sherman, E.; Soukiazian, S.; Verbrugge, M.; Tataria, H.; Musser, J.; Finamore, P. Cycle-life model for graphiteLiFePO$_4$ cells. *J. Power Sources* **2010**, *196*, 3942–3948. [CrossRef]
100. Todeschini, F.; Onori, S.; Rizzoni, G. An experimentally validated capacity degradation model for Li-ion batteries in PHEVs applications. *IFAC Proc. Vol.* **2012**, *45*, 456–461. [CrossRef]
101. Omar, N.; Monem, M.A.; Firouz, Y.; Salminen, J.; Smekens, J.; Hegazy, O.; Gaulous, H.; Mulder, G.; Van Den Bossche, P.; Coosemans, T.; et al. Lithium iron phosphate based battery—Assessment of the aging parameters and development of cycle life model. *Appl. Energy* **2014**, *113*, 1575–1585. [CrossRef]
102. Ecker, M.; Gerschler, J.B.; Vogel, J.; Käbitz, S.; Hust, F.; Dechent, P.; Sauer, D.U. Development of a lifetime prediction model for lithium-ion batteries based on extended accelerated aging test data. *J. Power Sources* **2012**, *215*, 248–257. [CrossRef]
103. Ouyang, M.; Feng, X.; Han, X.; Lu, L.; Li, Z.; He, X. A dynamic capacity degradation model and its applications considering varying load for a large format Li-ion battery. *Appl. Energy* **2016**, *165*, 48–59. [CrossRef]
104. Gao, Y.; Jiang, J.; Zhang, C.; Zhang, W.; Ma, Z.; Jiang, Y. Lithium-ion battery aging mechanisms and life model under different charging stresses. *J. Power Sources* **2017**, *356*, 103–114. [CrossRef]
105. Rezvanizaniani, S.M.; Liu, Z.; Chen, Y.; Lee, J. Review and recent advances in battery health monitoring and prognostics technologies for electric vehicle (EV) safety and mobility. *J. Power Sources* **2014**, *256*, 110–124. [CrossRef]
106. Hu, C.; Jain, G.; Zhang, P.; Schmidt, C.; Gomadam, P.; Gorka, T. Data-driven method based on particle swarm optimization and k-nearest neighbor regression for estimating capacity of lithium-ion battery. *Appl. Energy* **2014**, *129*, 49–55. [CrossRef]

107. Liu, D.; Zhou, J.; Liao, H.; Peng, Y.; Peng, X. A health indicator extraction and optimization framework for lithium-ion battery degradation modeling and prognostics. *IEEE Trans. Syst. Man Cybern. Syst.* **2015**, *45*, 915–928. [CrossRef]
108. Klass, V.; Behm, M.; Lindbergh, G. A support vector machine-based state-of-health estimation method for lithium-ion batteries under electric vehicle operation. *J. Power Sources* **2014**, *270*, 262–272. [CrossRef]
109. You, G.-W.; Park, S.; Oh, D. Real-time state-of-health estimation for electric vehicle batteries: A data-driven approach. *Appl. Energy* **2016**, *176*, 92–103. [CrossRef]
110. Kashkooli, A.G.; Fathiannasab, H.; Mao, Z.; Chen, Z. Application of artificial intelligence to state-of-charge and state-of-health estimation of calendar-aged lithium-ion pouch cells. *J. Electrochem. Soc.* **2019**, *166*, A605–A615. [CrossRef]
111. Mao, L.; Hu, H.; Chen, J.; Zhao, J.; Qu, K.; Jiang, L. Online state-of-health estimation method for lithium-ion battery based on CEEMDAN for feature analysis and RBF neural network. *IEEE J. Emerg. Sel. Top. Power Electron.* **2021**, *11*, 187–200. [CrossRef]
112. Lin, M.; Zeng, X.; Wu, J. State of health estimation of lithium-ion battery based on an adaptive tunable hybrid radial basis function network. *J. Power Sources* **2021**, *504*, 230063. [CrossRef]
113. Saha, B.; Goebel, K.; Poll, S.; Christophersen, J. Prognostics methods for battery health monitoring using a bayesian framework. *IEEE Trans. Instrum. Meas.* **2008**, *58*, 291–296. [CrossRef]
114. Zhang, S.; Zhai, B.; Guo, X.; Wang, K.; Peng, N.; Zhang, X. Synchronous estimation of state of health and remaining useful lifetime for lithium-ion battery using the incremental capacity and artificial neural networks. *J. Energy Storage* **2019**, *26*, 100951. [CrossRef]
115. Xia, Z.; Abu Qahouq, J.A. Lithium-ion battery ageing behavior pattern characterization and state-of-health estimation using data-driven method. *IEEE Access* **2021**, *9*, 98287–98304. [CrossRef]
116. Shi, Y.; Ahmad, S.; Tong, Q.; Lim, T.M.; Wei, Z.; Ji, D.; Eze, C.M.; Zhao, J. The optimization of state of charge and state of health estimation for lithium-ions battery using combined deep learning and Kalman filter methods. *Int. J. Energy Res.* **2021**, *45*, 11206–11230. [CrossRef]
117. Liu, Z.; Zhao, J.; Wang, H.; Yang, C. A new lithium-ion battery SOH estimation method based on an indirect enhanced health indicator and support vector regression in PHMs. *Energies* **2020**, *13*, 830. [CrossRef]
118. Feng, X.; Weng, C.; He, X.; Wang, L.; Ren, D.; Lu, L.; Han, X.; Ouyang, M. Incremental capacity analysis on commercial lithium-ion batteries using support vector regression: A parametric study. *Energies* **2018**, *11*, 2323. [CrossRef]
119. Guo, Y.; Huang, K.; Hu, X. A state-of-health estimation method of lithium-ion batteries based on multi-feature extracted from constant current charging curve. *J. Energy Storage* **2021**, *36*, 102372. [CrossRef]
120. Widodo, A.; Shim, M.-C.; Caesarendra, W.; Yang, B.-S. Intelligent prognostics for battery health monitoring based on sample entropy. *Expert Syst. Appl.* **2011**, *38*, 11763–11769. [CrossRef]
121. Cai, L.; Meng, J.; Stroe, D.-I.; Luo, G.; Teodorescu, R. An evolutionary framework for lithium-ion battery state of health estimation. *J. Power Sources* **2018**, *412*, 615–622. [CrossRef]
122. Yang, D.; Wang, Y.; Pan, R.; Chen, R.; Chen, Z. State-of-health estimation for the lithium-ion battery based on support vector regression. *Appl. Energy* **2018**, *227*, 273–283. [CrossRef]
123. Ma, C.; Zhai, X.; Wang, Z.; Tian, M.; Yu, Q.; Liu, L.; Liu, H.; Wang, H.; Yang, X. State of health prediction for lithium-ion batteries using multiple-view feature fusion and support vector regression ensemble. *Int. J. Mach. Learn. Cybern.* **2018**, *10*, 2269–2282. [CrossRef]
124. Xiong, W.; Mo, Y.; Yan, C. Online state-of-health estimation for second-use lithium-ion batteries based on weighted least squares support vector machine. *IEEE Access* **2020**, *9*, 1870–1881. [CrossRef]
125. Dai, H.; Wei, X.; Sun, Z.; Wang, J.; Gu, W. Online cell SOC estimation of Li-ion battery packs using a dual time-scale Kalman filtering for EV applications. *Appl. Energy* **2012**, *95*, 227–237. [CrossRef]
126. Lin, Q.; Wang, J.; Xiong, R.; Shen, W.; He, H. Towards a smarter battery management system: A critical review on optimal charging methods of lithium ion batteries. *Energy* **2019**, *183*, 220–234. [CrossRef]
127. Collin, R.; Miao, Y.; Yokochi, A.; Enjeti, P.; von Jouanne, A. Advanced electric vehicle fast-charging technologies. *Energies* **2019**, *12*, 1839. [CrossRef]
128. Zhang, R.; Xia, B.; Li, B.; Cao, L.; Lai, Y.; Zheng, W.; Wang, H.; Wang, W. State of the art of lithium-ion battery SOC estimation for electrical vehicles. *Energies* **2018**, *11*, 1820. [CrossRef]
129. Chaoui, H.; Ibe-Ekeocha, C.C. State of charge and state of health estimation for lithium batteries using recurrent neural networks. *IEEE Trans. Veh. Technol.* **2017**, *66*, 8773–8783. [CrossRef]
130. Zhang, Y.; Xiong, R.; He, H.; Shen, W. Lithium-ion battery pack state of charge and state of energy estimation algorithms using a hardwarein-the-loop validation. *IEEE Trans. Power Electron.* **2017**, *32*, 4421–4431. [CrossRef]
131. Chen, C.; Xiong, R.; Shen, W. A lithium-ion battery-in-the-loop approach to test and validate multiscale dual H infinity filters for state-of charge and capacity estimation. *IEEE Trans. Power Electron.* **2018**, *33*, 332–342. [CrossRef]

132. Tian, X.; Jeppesen, B.; Ikushima, T.; Baronti, F.; Morello, R. Accelerating State-Of-Charge Estimation in FPGA-based Battery Management Systems. In Proceedings of the 6th Hybrid and Electric Vehicles Conference (HEVC 2016), London, UK, 2–3 November 2016; pp. 4–6.
133. Sahinoglu, G.O.; Pajovic, M.; Sahinoglu, Z.; Wang, Y.; Orlik, P.V.; Wada, T. Battery state-of-charge estimation based on regular/recurrent gaussian process regression. *IEEE Trans. Ind. Electron.* **2017**, *65*, 4311–4321. [CrossRef]
134. Zhao, L.; Yao, W.; Wang, Y.; Hu, J. Machine learning-based method for remaining range prediction of electric vehicles. *IEEE Access* **2020**, *8*, 212423–212441. [CrossRef]
135. Zhu, S.; Han, J.; An, H.-Y.; Pan, T.-S.; Wei, Y.-M.; Song, W.-L.; Chen, H.-S.; Fang, D. A novel embedded method for in-situ measuring internal multi-point temperatures of lithium ion batteries. *J. Power Sources* **2020**, *456*, 227981. [CrossRef]
136. Peng, J.; Zhou, X.; Jia, S.; Jin, Y.; Xu, S.; Chen, J. High precision strain monitoring for lithium ion batteries based on fiber Bragg grating sensors. *J. Power Sources* **2019**, *433*, 226692. [CrossRef]
137. Teoh, E.J.; Tan, K.C.; Xiang, C. Estimating the number of hidden neurons in a feedforward network using the singular value decomposition. *IEEE Trans. Neural Netw.* **2006**, *17*, 1623–1629. [CrossRef]
138. Cui, Z.; Wang, L.; Li, Q.; Wang, K. A comprehensive review on the state of charge estimation for lithium-ion battery based on neural network. *Int. J. Energy Res.* **2021**, *46*, 5423–5440. [CrossRef]
139. Shen, S.; Sadoughi, M.; Li, M.; Wang, Z.; Hu, C. Deep convolutional neural networks with ensemble learning and transfer learning for capacity estimation of lithium-ion batteries. *Appl. Energy* **2020**, *260*, 114296. [CrossRef]
140. Li, Y.; Zou, C.; Berecibar, M.; Nanini-Maury, E.; Chan, J.C.-W.; Bossche, P.v.D.; Van Mierlo, J.; Omar, N. Random forest regression for online capacity estimation of lithium-ion batteries. *Appl. Energy* **2018**, *232*, 197–210. [CrossRef]
141. Xu, H.; Peng, Y.; Su, L. Health state estimation method of lithium ion battery based on NASA experimental data set. *IOP Conf. Ser. Mater. Sci. Eng.* **2018**, *452*, 032067. [CrossRef]
142. Kollmeyer, P. Panasonic 18650PF li-ion battery data. In *Mendeley Data*; Elsevier Inc: Amsterdam, The Netherlands, 2018; Volume 1. [CrossRef]
143. Naguib, M.; Kollmeyer, P.; Skells, M. LG 18650hg2 li-ion battery data and example deep neural network xEV SOC estimator script. *Mendeley Data* **2020**, *3*, 2020. [CrossRef]
144. Saha, K.; Goebel, B. *Battery Data Set. NASA Ames Prognostics Data Repository*; NASA Ames: Moffett Field, CA, USA, 2007. Available online: http://ti.arc.nasa.gov/project/prognostic-data-repository (accessed on 12 January 2025).
145. Feng, X.; Chen, J.; Zhang, Z.; Miao, S.; Zhu, Q. State-of-charge estimation of lithium-ion battery based on clockwork recurrent neural network. *Energy* **2021**, *236*, 121360. [CrossRef]
146. Yang, F.; Song, X.; Xu, F.; Tsui, K.-L. State-of-charge estimation of lithium-ion batteries via long short-term memory network. *IEEE Access* **2019**, *7*, 53792–53799. [CrossRef]
147. Bhattacharjee, A.; Verma, A.; Mishra, S.; Saha, T.K. Estimating state of charge for xEV batteries using 1D convolutional neural networks and transfer learning. *IEEE Trans. Veh. Technol.* **2021**, *70*, 3123–3135. [CrossRef]
148. Kim, S.; Choi, Y.Y.; Kim, K.J.; Choi, J.-I. Forecasting state-of-health of lithium-ion batteries using variational long short-term memory with transfer learning. *J. Energy Storage* **2021**, *41*, 102893. [CrossRef]